

Unveiling hidden features of social evolution by inferring Langevin dynamics from data

Youngkyoung Bae¹, Hajime Shimao², Seungwoong Ha³, Luna Yang⁴, and

David Wolpert^{*3, 5, 6, 7}

¹Department of Physics and Astronomy & Center for Theoretical Physics, Seoul National University, Seoul 08826, Korea

²Great Valley School of Professional Studies, Penn State, Malvern, Pennsylvania 19355

³Santa Fe Institute, Santa Fe, NM 87501, USA

⁴Department of Business and Economics, Pennsylvania State University Brandywine Campus, Media, PA 19063, USA

⁵Complexity Science Hub, Vienna

⁶Arizona State University, Tempe, AZ, USA

⁷International Center for Theoretical Physics, Trieste, Italy

Abstract

Are there hidden dynamical common patterns in the evolution of social and cultural history? While the growing availability of digitized social data invites us to answer this question, prevailing quantitative methods often rely on deterministic snapshots or average effects. Such approaches overlook the continuous and inherently uncertain nature of historical trajectories. In this paper, we propose a framework for modeling historical dynamics as stochastic processes described by stochastic differential equations (SDEs). By viewing historical change through the lens of continuous-time dynamics, this framework provides a natural language to describe how structural trends and inherent random fluctuations interact to shape societal evolution. This approach allows us to handle the uncertainty in fragmentary historical records, moving beyond the dichotomy of structural determinism versus pure chance. We demonstrate that adopting this stochastic perspective unlocks a rich suite of analytical capabilities unavailable to static models. Specifically, we introduce methods to: (1) quantify the irreversibility; (2) detect exogenous perturbations; (3) perform multiple imputation for missing historical records. This framework offers a unified methodology for dissecting the stability, contingency, and dynamics of historical change.

*Corresponding author: david.h.wolpert@gmail.com

Contents

1	Introduction	4
2	Stochastic Process Framework	6
2.1	State space design from historical observations	7
2.2	Stochastic differential equation (SDE) modeling	9
3	Advantages of SDE framework	11
3.1	Irreversibility: the arrow of history	11
3.2	Exogenous perturbation	13
3.3	Probabilistic imputation of missing data	14
4	Methodology for SDE inference	15
4.1	Langevin Bayesian Networks (LBN)	16
4.2	Nonparametric Gaussian process SDE (npSDE)	17
5	Application 1: Evolution of Political Economy	17
5.1	Construction of the state space	17
5.2	Inferring stochastic dynamics	18
5.3	Irreversibility	21
5.4	Exogenous perturbation detection	22
6	Application 2: Historical Civilizations	23
6.1	Construction of the state space	23
6.2	Global dynamics of scale and computation	24
6.3	Paris Basin: a directional shift toward computational capacity	25
6.4	Latium: institutional takeoff versus imperial contraction	31
6.5	Middle Yellow River Valley: sustained drift with episodic contractions and periodization signals	32
6.6	Other regions and overall patterns: anomalies as prompts for targeted inquiry	33
7	Discussion	34
7.1	Limitations in data quality and dynamics identifications	34
7.2	Homogeneity and independence assumptions	35
7.3	State space design and interpretability	36
7.4	Relative advantages of SDE fitting methodologies	36

7.5	Interpretation of Statistical regularities and Causal mechanisms	37
7.6	The meaning of stochastic explanation in social science	38
7.7	Outlook	39
Appendix A SDE Inference Methods		46
A.1	Langevin Bayesian Networks (LBN)	46
A.1.1	Approximation of Kramers-Moyal Coefficients	47
A.1.2	Network architectures	48
A.2	Nonparametric Gaussian process SDE (npSDE)	48
A.2.1	Gaussian process priors for drift and diffusion	48
A.2.2	Simulation-based likelihood and sparse, irregular data	49
A.2.3	Sensitivity equations and gradient-based optimization	50
Appendix B Dataset Description		51
B.1	Application 1: Evolution of Political Economy	51
B.2	Application 2: Historical Civilizations	52
Appendix C Additional Results		53
C.1	Epistemic uncertainty in Application 1	53

1 Introduction

The problem of historical change has occupied scholars since Thucydides and remains unresolved. Whether large-scale outcomes are shaped primarily by structural forces (e.g., demography, technology, institutions) or by contingent events and individual agency has long been debated across social sciences.¹ Building on this intuition, economists and historical sociologists have formalized the idea of path dependence, showing how small, often accidental perturbations can lock societies into trajectories that persist long after the initial conditions have been forgotten [2, 3]. Yet, the dominant empirical apparatus in quantitative history and political economy remains curiously static. Cliometrics, for all its achievements in bringing rigor to economic history [4], has tended to privilege regression-based methods designed to isolate average causal effects rather than to characterize the distribution of possible historical trajectories. The canonical tools of the contemporary “credibility revolution” [5], such as difference-in-differences, regression discontinuities, and instrumental variables, are powerful for adjudicating whether an intervention shifts an outcome *in expectation*. However, they offer limited information on the higher-order features that matter most in historical interpretation: the variability of historical paths, the accumulation of uncertainty over time, or the degree to which any realized trajectory should be regarded as typical or exceptional relative to the space of counterfactual possibilities. In this paper, we argue that stochastic dynamical models provide a complementary language for studying historical dynamics: one that moves beyond the dichotomy between “everything has a structural explanation” and “everything is just chance,” and instead decomposes historical evolution into systematic drift and irreducible fluctuation, thereby quantifying when and where trajectories are channeled by structural constraints and when they are meaningfully contingent [6, 7].

A stochastic model delivers not only a point prediction of how a system is expected to evolve, but also a full distribution of feasible transitions, thus making uncertainty an explicit object of analysis rather than a residual to be ignored [8]. This distinction is crucial in historical applications where long-run development reflects the interaction of persistent structural forces with episodic shocks that can permanently redirect trajectories. By contrast, a conventional regression of economic growth on democracy or inequality identifies an expected growth rate conditional on covariates, allowing for the nonlinearities suggested by the Kuznets curve [9]. However, it leaves unanswered how much variability remains in the system, how that variability depends on the current state, or how uncertainty accumulates over multi-decade horizons.² More fundamentally, such reduced-form approaches typically confound two conceptually distinct sources of uncertainty: *aleatoric*

¹Marx insisted that “men make their own history, but they do not make it as they please; they do not make it under self-selected circumstances, but under circumstances existing already, given and transmitted from the past” [1].

²Acemoglu and Robinson [10] emphasize that canonical accounts struggle to rationalize nondemocratic development paths, most notably the combination of sustained growth and limited or delayed democratization observed in parts of East Asia, highlighting the limits of mean-based reduced-form predictions.

uncertainty, arising from intrinsic randomness driven by hidden degrees of freedom (e.g., fluctuations in harvest yields due to local weather or the aggregate variability of individual economic decisions), and *epistemic* uncertainty, arising from our incomplete information, missing observations, measurement error, and model misspecification [11, 12]. In historical data, where records are fragmentary and measurement error is substantial, explicitly representing and distinguishing these sources of uncertainty is not a methodological embellishment; it is essential for disciplined inference about dynamics, contingency, and institutional change.

In this paper, we propose a framework for modeling historical systems as stochastic processes in continuous time. Concretely, we treat the state of a society—comprising variables such as population, territorial extent, complexity of institutions, or income inequality—as a vector evolving according to a stochastic differential equation (SDE). The *drift* term encodes the average “trend” of the system, while the *diffusion* term captures the local amplitude and structure of random fluctuations. This framework directly accommodates both aleatoric uncertainty (through the diffusion) and epistemic uncertainty (through posterior uncertainty about the drift and diffusion themselves). Furthermore, it does so in a way that is naturally tailored to panel or time-series data with irregular observation times, missing entries, and heterogeneous measurement quality. First-order Markov dynamics are a particularly attractive baseline in this setting: they are interpretable (“what happens next depends on where you are now”), relatively parsimonious, and often sufficient given the limited temporal resolution and sample sizes typical in historical datasets. Crucially, by focusing on the conditional transition densities, rather than long-run stationary distributions or equilibrium outcomes, stochastic process models allow us to extract as much information as possible from the dynamics that are actually observed.

Our main contribution is to demonstrate that fitting SDE models to historical data unlocks a rich suite of analytical capabilities unavailable to static models. First, we introduce a measure of *irreversibility*, based on likelihood ratios between forward and time-reversed trajectories, that quantifies the “arrow of history.” Using this metric, we verify the existence of a persistent average directionality in historical evolution. Furthermore, by resolving this measure over time, we assess the contribution of specific observed transitions to the arrow of history, distinguishing steps that follow the system’s structural tendency from those that move against the prevailing current. Second, we develop an *exogenous perturbation detector* that identifies dynamical anomalies, defined as transitions that deviate significantly from the system’s intrinsic trends and fluctuations. We interpret these anomalies as evidence of exogenous shocks or omitted variables, such as pandemics, exceptional leaders, or technological breakthroughs. This provides a principled method for identifying what Scheidel terms “great levelers” or the violent disruptions (e.g., warfare, revolution, state collapse, plague) that have historically driven major redistributions and institutional ruptures [13]. Crucially, because our models quantify epistemic uncertainty, we can distinguish genuinely surprising events from those surprising

only due to poor model constraints.

We apply our framework to two distinct domains, employing two complementary inference methods: Langevin Bayesian Networks (LBN) [14] and nonparametric Gaussian process stochastic differential equation (npSDE) [15] estimators. First, we analyze the joint dynamics of the modern political economy, comprising democracy, economic inequality, and economic growth. By inferring the governing SDE via the LBN method, we identify systematic trends and intrinsic volatility characteristics of different political-economic states. We also quantify irreversible trends and systematically detect exogenous perturbations in historical trajectories. Second, we model the development of historical civilizations using the Seshat databank [16] via the npSDE method. This allows us to quantitatively study civilizational ‘rise and fall,’ distinguishing between endogenous dynamic cycles and irreversible structural shifts, and assessing the detectability of major shocks such as the Bronze Age collapse. Across these applications, we show that treating historical data as realizations of an underlying stochastic process yields insights that are difficult to obtain from conventional linear or purely deterministic models. We can quantify when and where history behaves like a predictable trend plus small fluctuations, when and where it is dominated by intrinsic randomness, and when we see clear fingerprints of exogenous shocks or exceptional agents. We can identify which aspects of development are effectively one-way and which can be undone, and we can give a rigorous meaning to claims about “exceptionalism” by measuring how atypical an entire trajectory is under the dynamics that govern other units. Although our empirical examples are necessarily constrained by data limitations, the conceptual framework is general and can be applied to a wide range of historical and social-scientific questions.

The remainder of the paper is organized as follows. Section 2 establishes our stochastic process framework, clarifying the distinction between aleatoric and epistemic uncertainty and justifying the use of SDEs for historical data. Section 3 introduces the capabilities unlocked by this framework, formalizing the measures for time irreversibility, exogenous perturbation detection, and probabilistic imputation. Section 4 details the inference methodologies, describing both the Langevin Bayesian Networks (LBN) and the nonparametric Gaussian process SDE (npSDE) estimator. We then present our empirical findings: Section 5 analyzes the evolution of the modern political economy, while Section 6 examines the dynamics of historical civilizations using the Seshat dataset. Finally, Section 7 discusses data limitations and broader implications for debates on structure, contingency, and agency in history.

2 Stochastic Process Framework

To model historical change as a stochastic process, it is necessary to first clarify what constitutes the state of the system and how that state is assumed to evolve over time [6]. Historical observations are

fragmentary, heterogeneous in their sources, and irregularly sampled. Furthermore, many critical dimensions of social dynamics correspond to latent constructs, such as democracy and social complexity, that are not directly measured but theoretically constructed and only indirectly linked to observable indicators [17, 18]. Consequently, these records cannot be treated as direct realizations of a well-defined dynamical system. Instead, we adopt a latent-state perspective in which the observed historical record is viewed as an incomplete and noisy manifestation of an underlying continuous-time process [19, 20]. In this view, the latent state is not identified with a raw observed indicator, but is treated as a constructed macroscopic variable representing the effective dynamical conditions of the society. This approach allows us to bridge the gaps between discrete historical events by assuming a persistent, albeit hidden, dynamical continuity.

Within this framework, the object of interest is not a single realized trajectory, but the process governing the evolution of the latent state over time. Even under a latent-state perspective, the constructed macroscopic state cannot fully recover all degrees of freedom that shape social dynamics, particularly those that operate at faster timescales (e.g., microscopic interactions between individuals) or remain systematically unobserved. The reduction of such high-dimensional complexity into a structured state space necessarily introduces stochasticity [21]. Modeling this evolution as a stochastic process provides a principled way to represent such intrinsic variability, rather than treating it as measurement error or ignoring it altogether. A standard mathematical representation of such stochastic processes is given by stochastic differential equations (SDEs), in which the evolution of the state is decomposed into a *drift* term and a *diffusion* term [22]. Here, the former captures the average tendency of change conditional on the current state, while the latter characterizes the scale of stochastic fluctuations around this average. It is important to note that the inferred SDE should be interpreted with care, as it may otherwise be read as a universal deterministic law governing all societies. Instead, it provides a continuous-time description of the averaged common tendencies and dispersion observed across historical trajectories in the constructed state space (we return to this further in Sec. 7.5). To operationalize this framework, we first address the challenge of mapping heterogeneous records into a coherent state space (Sec. 2.1), followed by the formalization of the governing SDE (Sec. 2.2).

2.1 State space design from historical observations

The construction of a quantitative latent state space constitutes a foundational step in operationalizing the stochastic framework. To apply SDE-based inference, the historical state must be represented as a vector in a continuous state space where differential calculus applies. While certain historical indicators, such as polity population, income inequality (e.g., Gini coefficient), or economic output (e.g., real GDP), naturally exist in numerical forms, most of the critical dimensions of social dynamics do not. Even in comprehensive datasets

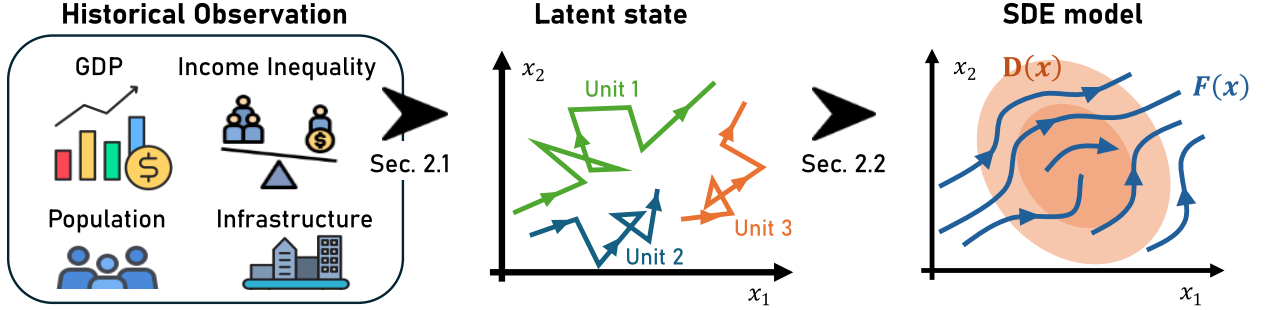


Figure 1: Conceptual overview of the framework. (Left) We start with historical raw observations (e.g., GDP, population) from multiple units. (Middle) These observations are represented as low-dimensional latent state trajectories (e.g., trajectories of Units 1, 2, and 3) evolving stochastically over time. (Right) The underlying dynamics of these latent states are modeled by an SDE, characterized by a drift field $\mathbf{F}(\mathbf{x})$ (blue arrows) and a diffusion matrix $\mathbf{D}(\mathbf{x})$ (orange ellipses), which we aim to infer.

like *Seshat: Global History Databank* [16], key variables defining money system, governance, or institutional capacity are frequently coded as categorical or ordinal values. These discrete codes reflect the granularity of historical sources, imperfectly capturing the evolution of the underlying society. Therefore, extracting continuous latent representation from these discrete proxies is essential, a feasibility demonstrated by prior quantitative studies [23, 24].

To enable this extraction, constructing a continuous state space first requires mapping qualitative information onto a quantitative scale, guided by theoretical constructs and domain knowledge [17]. Furthermore, even when numerical indicators are available, the raw variables are often sparse, high-dimensional, and heterogeneous. Directly using raw variables may lead to an ill-posed inference problem due to the curse of dimensionality and the noise inherent in historical recording. Therefore, it is often necessary to employ dimensionality reduction or latent variable models to project these fragmentary observations into a lower-dimensional, dynamically coherent representation. This latent-state construction ensures that the resulting state space is not only comparable across different historical units but also mathematically suitable for the continuous-time evolution described by SDEs.

Specifically, the operational pipeline for constructing the state space proceeds in three stages. First, raw indicators that span multiple orders of magnitude (e.g., population sizes or GDP) are log-transformed. This step is essential to address the heteroskedastic nature of historical growth; it ensures that stochastic fluctuations are modeled relative to the scale of the system (multiplicative noise) rather than its absolute size, thereby mitigating scale-dependent variance artifacts. Second, to handle the high dimensionality and collinearity of the transformed indicators, we employ dimensionality reduction techniques such as Principal Component Analysis (PCA) or Factor Analysis (FA). This projection aggregates correlated proxies into a compact set of orthogonal axes, effectively filtering out idiosyncratic noise associated with individual

sources. Finally, these extracted latent dimensions are interpreted as the *macro-variables* of the system (e.g., democracy index or aggregate social complexity). The resulting low-dimensional vector, denoted as $\mathbf{x}_t \in \mathbb{R}^d$ with dimensionality d , constitutes the effective macroscopic state of the system at time t .

2.2 Stochastic differential equation (SDE) modeling

Let us consider a d -dimensional stochastic process with a latent state \mathbf{x}_t that governs the system's dynamics. We assume that the dataset consists of N different units (e.g., countries or cities), indexed by $i = 1, \dots, N$. Although the observations are discrete in time, we model the underlying dynamics as evolving continuously according to the following stochastic differential equation (Itô convention) [22]:

$$d\mathbf{x}_t^{(i)} = \mathbf{F}(\mathbf{x}_t^{(i)})dt + \sqrt{2\mathbf{D}(\mathbf{x}_t^{(i)})} d\mathbf{W}_t^{(i)}, \quad (1)$$

where $d\mathbf{x}_t^{(i)} \equiv \mathbf{x}_{t+dt}^{(i)} - \mathbf{x}_t^{(i)}$ is the change of state $\mathbf{x}_t^{(i)}$ during an infinitesimal time interval dt , $\mathbf{F} : \mathbb{R}^d \rightarrow \mathbb{R}^d$ is the drift vector field representing the deterministic trend, and $\mathbf{D} : \mathbb{R}^d \rightarrow \mathbb{R}^{d \times d}$ is the state-dependent diffusion matrix representing the magnitude and covariance structure of stochastic fluctuations. This formulation decomposes the historical change into a structural force (\mathbf{F}) and intrinsic volatility (\mathbf{D}). Here, $\mathbf{W}_t^{(i)}$ is a standard d -dimensional Wiener process independent across units, with increments $d\mathbf{W}_t^{(i)}$ having zero mean and covariance $\mathbf{I}_d dt$ where \mathbf{I}_d denotes the $d \times d$ identity matrix. Crucially, we assume that all units follow common underlying dynamics governed by \mathbf{F} and \mathbf{D} , allowing us to infer these shared functions from the aggregated trajectories of the ensemble. For the sake of notational brevity, we will hereafter omit the unit index (i) when referring to the general dynamics, unless a specific distinction between units is required.

To clarify the physical meaning of these terms, consider the state change $\delta\mathbf{x}_t \equiv \mathbf{x}_{t+\delta t} - \mathbf{x}_t$ over a small time interval δt . By discretizing Eq. (1) through Euler–Maruyama approximation, we obtain:

$$\delta\mathbf{x}_t = \mathbf{F}(\mathbf{x}_t)\delta t + \sqrt{2\mathbf{D}(\mathbf{x}_t)} \delta\mathbf{W}_t + \mathcal{O}(\delta t^2), \quad (2)$$

where $\delta\mathbf{W}_t \equiv \mathbf{W}_{t+\delta t} - \mathbf{W}_t$ has zero mean and covariance $\mathbf{I}_d \delta t$. Note that the validity of the approximation in Eq. (2) relies on the time step δt being sufficiently small. Historical datasets, however, are often irregularly and sparsely sampled, with potentially large observation gaps (e.g., the observation interval $\Delta t^{\text{obs}} \simeq 100$ years in the Seshat dataset [16]). In this setting, directly substituting the observation interval Δt^{obs} for δt in Eq. (2) can lead to large approximation errors. Accordingly, we distinguish the physical observation interval Δt^{obs} from the numerical time step used to approximate the continuous-time dynamics. To bridge these scales, we employ a flexible time transformation. First, the observed time t^{obs} is mapped to a simulation time

t via the rescaling $t = \alpha t^{\text{obs}}$, where $\alpha > 0$ is a scaling factor, so that the observation interval in the simulation clock becomes $\Delta t = \alpha \Delta t^{\text{obs}}$. Second, depending on the inference method (e.g., simulation-based likelihood), this rescaled interval Δt can be further partitioned into N_{sub} sub-steps to ensure numerical stability. In this case, the effective numerical integration step is defined as $\delta t \equiv \Delta t / N_{\text{sub}}$. This two-stage approach, rescaling followed by optional sub-stepping, ensures that the numerical step δt remains sufficiently small for an accurate Euler–Maruyama approximation, regardless of the sparsity of the original historical data.

Based on Eq. (2), the transition probability density for observing a displacement $\delta \mathbf{x}_t$ given the current state \mathbf{x}_t can be approximated as a Gaussian distribution (Onsager–Machlup functional in Itô convention) [25]:

$$\begin{aligned} P(\delta \mathbf{x}_t \mid \mathbf{x}_t) &\approx \mathcal{N}(\delta \mathbf{x}_t \mid \mathbf{F}(\mathbf{x}_t) \delta t, 2\mathbf{D}(\mathbf{x}_t) \delta t) \\ &\propto \exp \left[-\frac{1}{4\delta t} (\delta \mathbf{x}_t - \mathbf{F}(\mathbf{x}_t) \delta t)^\top \mathbf{D}(\mathbf{x}_t)^{-1} (\delta \mathbf{x}_t - \mathbf{F}(\mathbf{x}_t) \delta t) \right], \end{aligned} \quad (3)$$

where $\mathcal{N}(\mathbf{z} \mid \boldsymbol{\mu}_{\mathbf{z}}, \boldsymbol{\Sigma}_{\mathbf{z}})$ denotes the multivariate Gaussian distribution of \mathbf{z} with mean $\boldsymbol{\mu}_{\mathbf{z}}$ and covariance $\boldsymbol{\Sigma}_{\mathbf{z}}$. Eq. (3) indicates that the probability of transitioning to the next state is determined solely by the current state, which characterizes the Markov property. From this transition density, we explicitly recover the statistical moments of the state change $\delta \mathbf{x}_t$ (i.e., Kramers–Moyal coefficients) [25]:

$$\langle \delta \mathbf{x}_t \mid \mathbf{x}_t \rangle \approx \mathbf{F}(\mathbf{x}_t) \delta t, \quad \text{Cov}[\delta \mathbf{x}_t \mid \mathbf{x}_t] \approx 2\mathbf{D}(\mathbf{x}_t) \delta t, \quad (4)$$

This relation identifies the drift and diffusion matrix as the first and second conditional moments, respectively, forming the theoretical basis for various SDE inference methods [26]. We note that, in simulation-based SDE inference, Eq. (3) is applied at the internal discretization level, and the finite-time transition over Δt is obtained by composing these small-step transitions via numerical simulation. Building on this property, the probability of a trajectory $\Gamma \equiv \{\mathbf{x}_{t_0}, \mathbf{x}_{t_1}, \dots, \mathbf{x}_{t_L}\}$ is given by the product of the initial probability p_0 and the subsequent transition probabilities:

$$\mathcal{P}[\Gamma] = p_0(\mathbf{x}_{t_0}) \prod_{k=0}^{L-1} P(\mathbf{x}_{t_{k+1}} \mid \mathbf{x}_{t_k}) \quad (5)$$

where $P(\mathbf{x}_{t_{k+1}} \mid \mathbf{x}_{t_k})$ is equivalent to the displacement density $P(\Delta \mathbf{x}_{t_k} \mid \mathbf{x}_{t_k})$ with $\Delta \mathbf{x}_{t_k} \equiv \mathbf{x}_{t_{k+1}} - \mathbf{x}_{t_k}$. This path probability formulation serves as the foundation for quantifying the time irreversibility of the system, which typically involves comparing the likelihood of a forward trajectory $\mathcal{P}[\Gamma]$ with that of its time-reversed counterpart (see Sec. 3.1).

Finally, we highlight two key theoretical assumptions underpinning this framework:

Markovianity and hidden variables. Our SDE formulation relies on the Markov assumption, meaning that the instantaneous state \mathbf{x}_t contains sufficient information to determine the future evolution of the system. In practice, however, the constructed latent state may omit essential *slow* variables that influence the dynamics. In such cases, the resulting effective dynamics can exhibit memory effects, making the process path-dependent and therefore non-Markovian [21, 27]. Our proposed framework can, in principle, be extended to higher-order formulations, such as second-order (i.e., underdamped) Langevin equations or Generalized Langevin Equations with memory kernels, to explicitly account for non-Markovianity. Nevertheless, applying these more complex models demands a substantially larger volume of data than what is typically available in historical records. Moreover, historical records are often sampled at coarse temporal resolutions (e.g., annual to centennial), which may exceed fast relaxation times such as momentum relaxation, making a Markov approximation reasonable at the observation scale [25]. We therefore adopt a first-order approximation (i.e., overdamped Langevin equation) in this study as written in Eq. (1) and assess the validity of this assumption within the latent state space. Specifically, we examine the temporal correlation of inferred noise. As demonstrated in Sec. 5, the residuals are approximately uncorrelated in time, which is consistent with the Markovian approximation.

Gaussian white noise assumption. Modeling stochastic fluctuations as a Wiener process in Eq. (1) implies that the system dynamics are driven by Gaussian white noise, a common starting point for studying stochastic dynamics. This assumption is motivated by the fact that, in complex socio-economic systems, macroscopic fluctuations often arise from the aggregation of numerous microscopic events and individual decisions occurring on timescales much faster than the macroscopic evolution [28]. Under such a separation of timescales, the collective effect of many weakly dependent contributions is expected to converge toward Gaussian statistics by the Central Limit Theorem, while rapidly decorrelating perturbations justify a white-noise approximation. However, historical dynamics may still exhibit non-Gaussian features due to rare but impactful external shocks (e.g., wars and financial crises) that induce abrupt jumps. To account for this, we explicitly identify and quantify these events as *exogenous perturbations* in Sec. 3.2, treating them separately from the endogenous fluctuations represented by the Wiener process.

3 Advantages of SDE framework

3.1 Irreversibility: the arrow of history

Many macroscopic historical processes exhibit a distinct directionality or time-irreversibility. While random fluctuations look statistically identical whether time flows forward or backward, historical evolution follows a

distinct ‘arrow of time’, manifesting as persistent trends in economic growth, institutional complexity, or democratization. If we were to observe the history of political economy played in reverse, it would appear fundamentally different from its actual trajectory. To quantify this directionality, we adapt the concept of stochastic (medium) entropy production from non-equilibrium statistical mechanics and define the path irreversibility $\Sigma[\Gamma] \in \mathbb{R}$ for an observed trajectory $\Gamma \equiv \{\mathbf{x}_{t_0}, \dots, \mathbf{x}_{t_L}\}$ [29]:

$$\Sigma[\Gamma] \equiv \ln \frac{\mathcal{P}[\Gamma \mid \mathbf{x}_{t_0}]}{\mathcal{P}[\tilde{\Gamma} \mid \mathbf{x}_{t_L}]}, \quad (6)$$

where $\tilde{\Gamma} = \{\mathbf{x}_{t_L}, \dots, \mathbf{x}_{t_0}\}$ denotes the time-reversed counterpart of Γ . This quantity is closely related to stochastic entropy production in nonequilibrium statistical mechanics [30, 31] and measures the extent to which the inferred dynamics break time-reversal symmetry (i.e., violate detailed balance), thereby serving as a quantitative measure of nonequilibrium activity in many biological systems [32–34]. Thus, a non-zero Σ provides a quantitative measure of the *arrow of history*. Larger values of $|\Sigma|$ indicate more pronounced temporal asymmetry and greater statistical distinguishability from reversible random fluctuations.

For the stochastic process governed by the inferred SDE (1), the Markov property allows us to decompose $\Sigma[\Gamma]$ into a sum of local contributions:

$$\Sigma[\Gamma] = \sum_{k=0}^{L-1} \sigma_{t_k}. \quad (7)$$

where the local irreversibility σ_t is defined by

$$\sigma_t \equiv \ln \frac{P(\mathbf{x}_{t+\Delta t} \mid \mathbf{x}_t)}{P(\mathbf{x}_t \mid \mathbf{x}_{t+\Delta t})}. \quad (8)$$

Here, Δt denotes the effective transition interval used to evaluate the transition density, which may coincide with the observation interval or with an internal discretization step. While $\Sigma[\Gamma]$ quantifies the trajectory-wise irreversibility, representing the *cumulative* arrow of history for Γ , σ_t resolves this directionality at the transition level, defining the *local* arrow of history at each time t . Utilizing both metrics allows us to examine the alignment of the historical path and specific events with the system’s inferred directional tendency. In the inferred dynamics, $\sigma_t > 0$ indicates that the realized transition is statistically more consistent with the forward dynamics than with its time-reversed counterpart, whereas $\sigma_t < 0$ indicates the opposite. Importantly, this metric captures statistical directionality only; it does not assign normative or ethical value to the observed history. For instance, if the drift points toward democratic erosion in high-inequality regimes, then a decrease in democracy may yield positive irreversibility even though such a change may be normatively undesirable.

3.2 Exogenous perturbation

While irreversibility characterizes the directionality of a trajectory, it does not quantify how expected a specific transition is. Even a trajectory perfectly aligned with the arrow of history may experience sudden jumps that are statistically unlikely under the continuous SDE formulation. To address this, our framework enables a principled decomposition of historical fluctuations into endogenous and exogenous components. We first define *endogenous perturbations* as the stochastic fluctuations arising from the system's intrinsic dynamics, mathematically represented by the diffusion term $\sqrt{2\mathbf{D}(\mathbf{x}_t)}d\mathbf{W}_t$ in Eq. (1). These fluctuations capture the aggregated effect of microscopic degrees of freedom (e.g., harvest variability or individual economic decisions) that are inherent to the system's normal evolution [12]. Under this definition, a transition is considered normal or endogenous if it falls within the probabilistic envelope governed by the drift $\mathbf{F}(\mathbf{x})$ and diffusion $\mathbf{D}(\mathbf{x})$.

However, strictly disentangling true external shocks from rare tail events of the internal dynamics is often infeasible in complex historical systems. Consequently, rather than relying on a rigid causal classification, we operationalize *exogenous perturbations* through the lens of statistical improbability. We identify these perturbations as observed transitions that are highly unlikely (low-probability events) under the learned endogenous factors $\mathbf{F}(\mathbf{x})$ and $\mathbf{D}(\mathbf{x})$ [8]. In this framework, significant deviations from the distribution predicted by the governing SDE serve as proxies for external shocks that drive the system away from its structural trajectory (e.g., wars, revolutions, or radical institutional ruptures) [13]. To systematically quantify this improbability, we introduce a detection method based on the information-theoretic surprisal (or negative log-likelihood) of observed transitions.

For a single transition $\mathbf{x}_t \rightarrow \mathbf{x}_{t+\Delta t}$, the surprisal s_t is defined as the negative log-likelihood under the inferred dynamics:

$$s_t \equiv -\ln P(\mathbf{x}_{t+\Delta t} \mid \mathbf{x}_t). \quad (9)$$

This metric quantifies how unexpected a specific historical step is, given the structural trends (\mathbf{F}) and intrinsic volatility (\mathbf{D}) learned by our models. Here, we note that the computation of the transition probability $P(\mathbf{x}_{t+\Delta t} \mid \mathbf{x}_t)$ depends on the inference method and the time scale.

While this definition aligns with the concept of self-information [35], this raw surprisal conflates high intrinsic volatility (endogenous noise) with external shocks. Thus, it is difficult to distinguish whether a high s_t arises from the baseline endogenous randomness or from an exogenous perturbation. To filter out this baseline volatility, we define the *normalized surprisal* \tilde{s}_t by subtracting the local average of s_t :

$$\tilde{s}_t \equiv s_t - \langle -\ln P(\mathbf{x}' \mid \mathbf{x}_t) \rangle_{\mathbf{x}' \sim P(\cdot \mid \mathbf{x}_t)} \quad (10)$$

Equivalently, \tilde{s}_t measures whether the realized transition lies in the tail of the predictive distribution relative to the typical uncertainty level at \mathbf{x}_t , rather than merely reflecting a locally high diffusion magnitude. This metric quantifies how far the transition deviates from the expected motion relative to the system's intrinsic volatility.

3.3 Probabilistic imputation of missing data

Historical datasets often contain gaps: we may observe a state \mathbf{x}_0 at time t_0 and a state \mathbf{x}_T at a later time t_T , but nothing in between. Our stochastic process framework allows us to impute the missing intermediate states in a principled way by sampling from the conditional distribution $P(\mathbf{x}_t \mid \mathbf{x}_0, \mathbf{x}_T)$ with $t_0 < t < t_T$ governed by the learned SDE. Leveraging the Markov property, this smoothing distribution factorizes as:

$$P(\mathbf{x}_t \mid \mathbf{x}_0, \mathbf{x}_T) \propto P(\mathbf{x}_T \mid \mathbf{x}_t)P(\mathbf{x}_t \mid \mathbf{x}_0). \quad (11)$$

Since the normalization constant is intractable, we employ an *Importance Sampling* scheme to approximate this distribution:

1. **Proposal: simulate candidates from the forward dynamics.** We first generate S candidate states $\{\mathbf{x}_t^{(s)}\}_{s=1}^S$ by simulating the learned SDE forward from \mathbf{x}_0 up to time t . Concretely, we apply the Euler–Maruyama scheme with step size δt ,

$$\mathbf{x}_{u+\delta t}^{(s)} = \mathbf{x}_u^{(s)} + \mathbf{F}(\mathbf{x}_u^{(s)}) \delta t + \sqrt{2\mathbf{D}(\mathbf{x}_u^{(s)})} \delta \mathbf{W}_s,$$

starting from $\mathbf{x}_{t_0}^{(s)} = \mathbf{x}_0^{(s)}$ and iterating until $u = t$. The resulting $\mathbf{x}_t^{(s)}$ are approximate draws from the forward transition density $P(\mathbf{x}_t \mid \mathbf{x}_0)$.

2. **Weighting: evaluate compatibility with the endpoint.** For each candidate $\mathbf{x}_t^{(s)}$, we approximate the likelihood of the observed endpoint given that candidate,

$$P(\mathbf{x}_T \mid \mathbf{x}_t^{(s)}),$$

by propagating the SDE forward from $\mathbf{x}_t^{(s)}$ to t_T . When the remaining interval $t_T - t$ is short, a single Gaussian approximation of the form (3) suffices:

$$\mathbf{x}_T \approx \mathbf{x}_t^{(s)} + \mathbf{F}(\mathbf{x}_t^{(s)}) \Delta + \sqrt{2\mathbf{D}(\mathbf{x}_t^{(s)})} \varepsilon, \quad \varepsilon \sim \mathcal{N}(\mathbf{0}, \mathbf{I}_d \Delta),$$

with $\Delta = t_T - t$. For longer intervals, we discretize $[t, t_T]$ into smaller steps and either (i) apply the Euler–Maruyama scheme to obtain a Gaussian approximation with accumulated mean and covariance, or (ii) simulate short forward paths from $\mathbf{x}_t^{(s)}$ to t_T and estimate a kernel density at \mathbf{x}_T . In either case, we obtain an approximate value for $P(\mathbf{x}_T | \mathbf{x}_t^{(s)})$.

3. Resampling: approximate the bridge distribution. Using Eq. (11), we assign an importance weight

$$w_s \propto P(\mathbf{x}_T | \mathbf{x}_t^{(s)}),$$

to each candidate, noting that the proposal distribution is $P(\mathbf{x}_t | \mathbf{x}_0)$ by construction. We then normalize the weights so that $\sum_{s=1}^S w_s = 1$, and resample from $\{\mathbf{x}_t^{(s)}\}$ according to $\{w_s\}$. The resampled states are approximate draws from the target distribution $P(\mathbf{x}_t | \mathbf{x}_0, \mathbf{x}_T)$.

For longer gaps spanning multiple time steps, this procedure is naturally extended using Sequential Monte Carlo methods. Unlike simple linear interpolation, this probabilistic imputation reconstructs trajectories that respect the nonlinear vector fields and intrinsic volatility of historical dynamics.

4 Methodology for SDE inference

The primary challenge in this framework is the inverse problem: extracting the underlying SDE from sparse, noisy, and indirect historical observations. This problem is exacerbated by the fact that historical observations are typically heterogeneous and subject to substantial measurement uncertainty. This task is not unique to historical analysis; closely related inference problems arise in statistical physics, biology, and climate science, where governing dynamics are modeled as SDEs under partial observability. Over the past decades, these fields have developed a rich set of methodologies, ranging from classical binning [26, 36–38] and basis function projections [39–41] to kernel-based [15, 42] and neural network estimators [14, 43–45].

Despite this diversity, many existing methods are implicitly tailored to settings in which trajectories are densely sampled in time, or where strong prior knowledge about the functional form of the dynamics can be reasonably assumed; conditions that historical data systematically violate. First, historical time series are typically sparse, short, and irregularly sampled. Observation times often differ substantially across units and periods, long gaps are common, and the number of observations per trajectory is frequently too small to support reliable estimation of local transition statistics or asymptotic arguments based on long trajectories. Second, in contrast to many physical or biological systems, there is rarely strong theoretical guidance about the appropriate functional form of historical dynamics. While mechanistic interpretations may exist at a qualitative level, imposing specific parametric forms for the drift or diffusion risks hard-coding contested

assumptions about social processes into the model. As a result, inference strategies that rely on flexible function-space representations and explicit uncertainty quantification are particularly attractive in historical applications. Taken together, these considerations motivate a focus on SDE inference methods that can accommodate sparse and irregular observations, operate with limited data, and avoid strong parametric assumptions on functional form.

To demonstrate the versatility of our framework across different data regimes, we employ two complementary estimation strategies tailored to the specific characteristics of each application. For the analysis of the modern political economy (Application 1), where relative data abundance allows for capturing complex functional dependencies, we utilize the Langevin Bayesian Networks (LBN) [14]. Conversely, for the study of historical civilizations (Application 2), which is characterized by extreme sparsity and irregular sampling, we employ the nonparametric Gaussian process SDE (npSDE) estimator [15]. While these methods differ in their mathematical foundations, both share the critical ability to perform uncertainty-aware inference without imposing strong parametric assumptions. This strategic selection ensures that our inference remains robust and well-suited to the distinct limitations of each historical dataset. We refer the reader to Refs. [14, 15] and the Appendix for methodological details.

4.1 Langevin Bayesian Networks (LBN)

To capture highly nonlinear dynamics while rigorously quantifying epistemic uncertainty, we employ the Langevin Bayesian Network (LBN) framework. Fundamentally, this method employs distinct neural network estimators to approximate the drift $F(x)$ and diffusion $D(x)$, respectively. The training objective is formulated to match the network outputs with the first and second conditional moments, i.e., the Kramers-Moyal coefficients, defined in Eq. (4).

Specifically, we utilize Stochastic Weight Averaging-Gaussian (SWAG) [46] combined with k -fold cross-validation. Instead of relying on a single best-fit model, which is prone to overfitting on small historical datasets, this approach constructs an ensemble of models. By sampling network parameters from the approximate posterior distribution derived via SWAG, the method generates a distribution of predicted drifts and diffusions for any given state. The mean of this ensemble represents the most probable structural trend, while the variance quantifies the model's uncertainty arising from data sparsity. This uncertainty-aware architecture allows us to distinguish regions of the state space where the inferred dynamics are well-constrained by historical evidence from those where the model is extrapolating. Detailed network architectures and training protocols are provided in Appendix A.1.

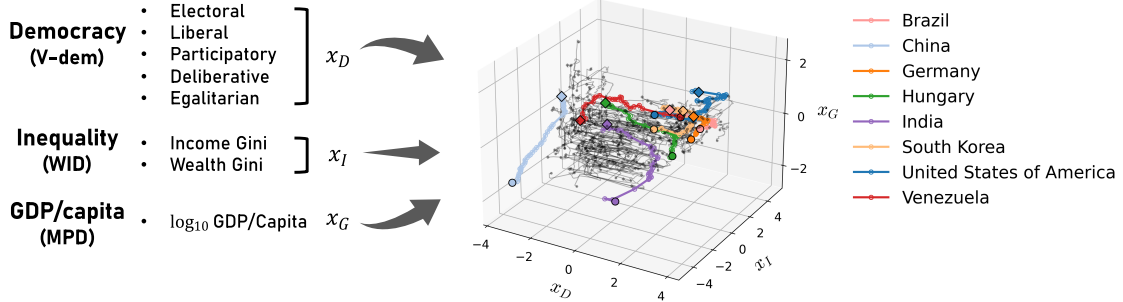


Figure 2: Trajectories of nations in the latent space of political economic development. The axes \mathbf{x}_D , \mathbf{x}_I , and \mathbf{x}_G represent the principal components corresponding to Democracy (V-Dem), Inequality (WID), and the logarithm of real GDP/capita (MPD) using 2011 purchasing power parities benchmark, respectively. Colored paths trace the historical evolution of representative countries, illustrating diverse developmental patterns. The circle denotes the starting year, and the diamond indicates the most recent year. Grey lines depict the trajectories of other countries.

4.2 Nonparametric Gaussian process SDE (npSDE)

As a complementary approach, we employ the nonparametric SDE (npSDE) estimator [15]. This method models the unknown drift and diffusion functions using Gaussian Processes (GPs), offering a flexible, data-driven representation without assuming a parametric functional form. A key advantage of npSDE for historical analysis lies in its simulation-based inference strategy. Rather than estimating derivatives directly from noisy data (gradient matching), which typically requires dense sampling, npSDE infers dynamics by simulating candidate paths from the current model and matching their distributions to the observed data points.

This generative approach makes the method particularly robust to the irregular sampling intervals and measurement noise characteristic of historical records. To ensure computational tractability, the method employs sparse inducing-point approximations, allowing the GP to scale effectively while maintaining the ability to capture local variations in the dynamics. The resulting posterior distribution over the drift and diffusion functions naturally provides confidence intervals for the inferred dynamics. Further details on the kernel specifications and the simulation-based likelihood optimization are described in Appendix A.2.

5 Application 1: Evolution of Political Economy

5.1 Construction of the state space

We define the macroscopic state of a society at observation year t^{obs} as a vector $\mathbf{x}_{t^{\text{obs}}} \equiv [x_D, x_I, x_G]^{\top} \in \mathbb{R}^3$, representing political democracy, economic inequality, and economic growth, respectively. To quantify these dimensions, we integrate data from three primary sources: the *Varieties of Democracy* (V-Dem) project [47], the *World Inequality Database* (WID) [48], and the *Maddison Project Database* (MPD) [49]. Specifically, the

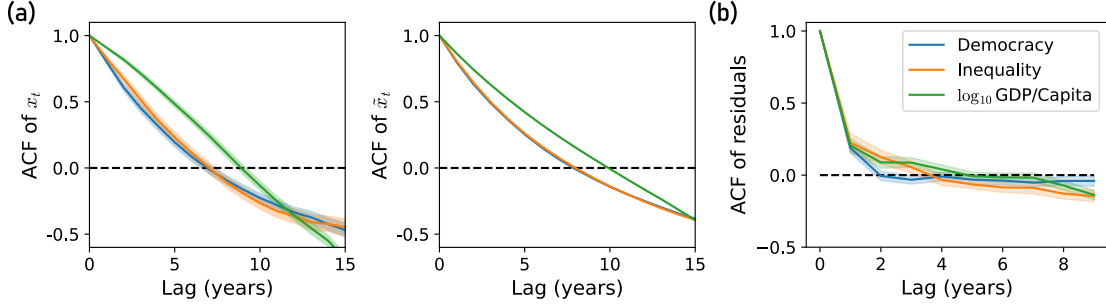


Figure 3: (a) Comparison of the Autocorrelation Function (ACF) between the observed historical data x_t (left) and the trajectories \tilde{x}_t generated from simulations of the inferred dynamics (right). (b) ACF of the standardized residuals $(2\mathbf{D}(\mathbf{x}_t))^{-1/2}(\Delta \mathbf{x}_t - \mathbf{F}(\mathbf{x}_t)\Delta t)$. The immediate drop to zero for all variables, Democracy (blue), Inequality (orange), and $\log_{10} \text{GDP/Capita}$ (green), indicates that the residuals are temporally uncorrelated (white noise), supporting the Markov assumption. Shaded regions indicate 95% confidence intervals in (a) and (b).

variables \mathbf{x}_D and \mathbf{x}_I are derived by applying Principal Component Analysis (PCA) to sets of standardized indicators from V-Dem and WID, respectively. We utilize the first principal component (PC1) for each dimension, oriented such that higher values of \mathbf{x}_D indicate stronger democratic institutions, and higher values of \mathbf{x}_I signify greater economic inequality. The economic growth dimension, \mathbf{x}_G , is defined as the standardized value of the logarithm of real GDP per capita to account for the exponential scale of aggregate production. To ensure numerical stability consistent with the framework described in Sec. 2, we rescale the physical time by a factor α , yielding an effective time step of $\Delta t = \delta t = 10^{-2}$.

The final dataset constitutes an unbalanced panel covering 149 countries with an annual resolution. While the longest time series spans from 1910 to 2022 (e.g., France) and shorter series begin as late as 2007 (e.g., Palestine-Gaza), the majority of countries are tracked from 1995 to 2022. Furthermore, the data are not strictly continuous and contain occasional missing years. To preserve the empirical signal and avoid potential artifacts, we do not apply any temporal interpolation to the raw data. Finally, consistent with the framework introduced in Sec. 2.2, we rescale the physical observation time t^{obs} (years) to the simulation time t used in the SDE inference. This is achieved by mapping the baseline annual interval to a dimensionless time step of $\Delta t = 10^{-2}$. Detailed descriptions of the dataset, PCA statistics, and preprocessing steps are provided in Appendix B.1.

5.2 Inferring stochastic dynamics

We apply the LBN framework (Sec. 4.1) to the constructed political economy dataset to infer the underlying drift field $F(x)$ and diffusion matrix $D(x)$. This allows us to decompose the evolution of political economy into deterministic structural trends and stochastic fluctuations.

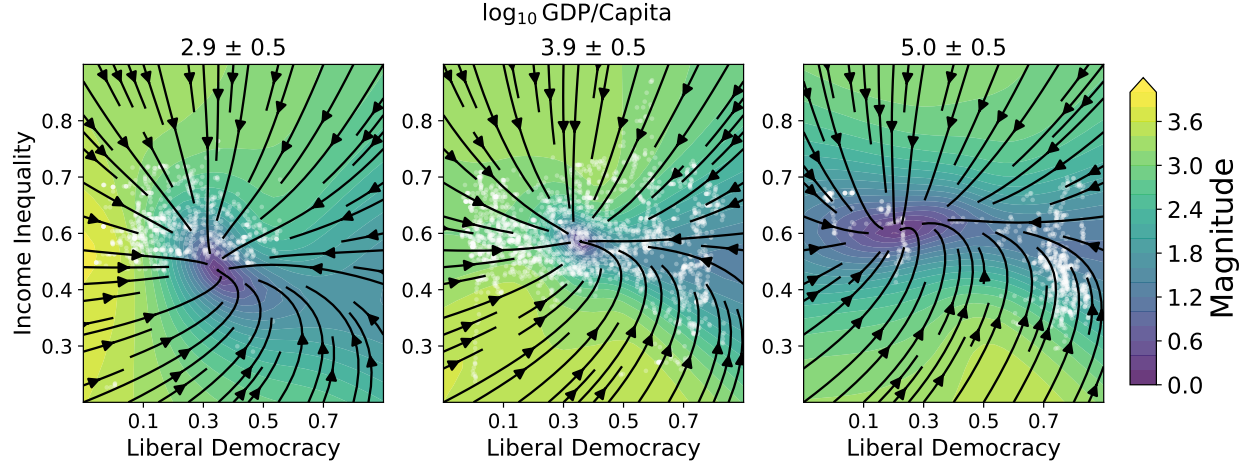


Figure 4: Inferred drift field $\mathbf{F}(\mathbf{x})$ on the Democracy-Inequality plane. Columns correspond to different ranges of $\log_{10}(\text{GDP}/\text{capita})$ (left to right: $2.9, 3.9, 5.0$). Black streamlines depict the mean drift field, the background color map indicates the magnitude $|\mathbf{F}(\mathbf{x})|$, and white dots represent the observed data points. The axes display values mapped from \mathbf{x} back to the original variable space via linear fitting for visualization.

Model Validation and Markovianity test Before analyzing the inferred dynamical landscapes, we validate the model’s ability to reproduce historical trajectories and assess the underlying Markov assumption. Figure 3 (a) compares the autocorrelation function (ACF) of the original historical data (left) with that of the trajectories generated by the inferred SDE (right). The decay patterns of the simulated trajectories closely match those of the observed data, confirming that the model successfully captures the temporal persistence and dynamical characteristics of the actual political economy. Furthermore, we examine whether the system is influenced by unobserved memory effects. Figure 3 (b) displays the ACF of the standardized residuals, calculated by normalizing the deviations from the deterministic drift (i.e., $(2\mathbf{D}(\mathbf{x}_t))^{-1/2}(\Delta\mathbf{x}_t - \mathbf{F}(\mathbf{x}_t)\Delta t)$). The correlations for all state variables drop rapidly to zero, indicating that the residual noise is effectively white noise. This lack of temporal correlation implies the absence of slow hidden variables, verifying that our three-dimensional state space is sufficient to describe the evolution of the system as a Markov process.

Inferred drift fields $\mathbf{F}(\mathbf{x})$. In Fig. 4, the inferred drift fields visualize the deterministic trajectories of the socio-economic system. The analysis identifies a distinct dynamical valley in high-inequality regions, where streamlines consistently align toward lower democracy scores. This structure confirms that the model correctly captures the destabilizing pressure of inequality on democratic institutions, aligning with recent findings [50], which demonstrate that high economic inequality serves as a strong predictor of democratic erosion.

Crucially, our framework reveals how economic development reshapes this landscape. In lower GDP contexts (left panel), the drift directs the system toward a sink at moderate democracy levels, indicating a residual restoring force. However, as GDP increases, this resilience diminishes. In high-GDP contexts

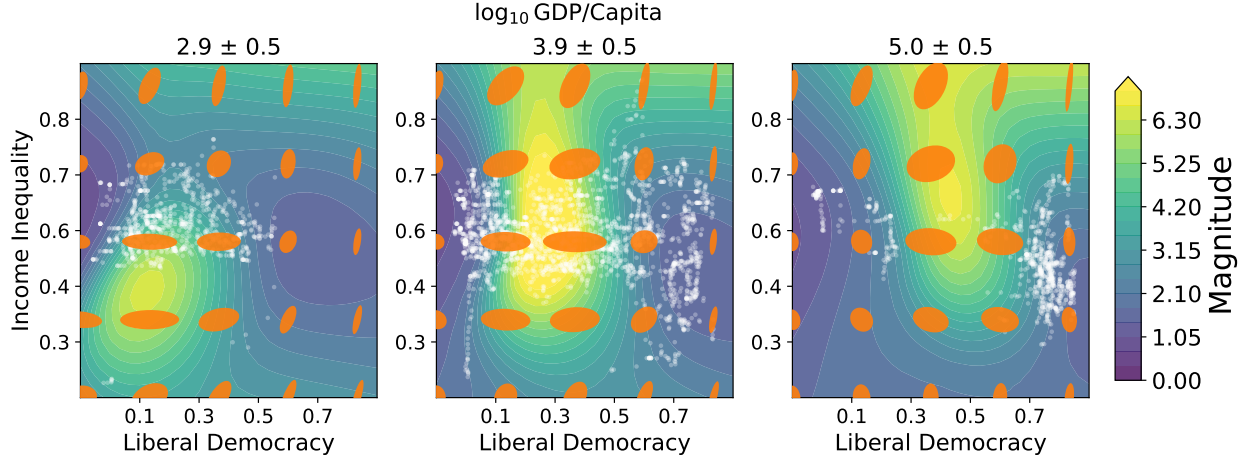


Figure 5: Inferred diffusion field $\mathbf{D}(\mathbf{x})$ on the Democracy-Inequality plane. Columns correspond to different ranges of $\log_{10}(\text{GDP/capita})$ (left to right: $2.9, 3.9, 5.0$). Orange ellipses depict the local diffusion anisotropy, where the orientation and size correspond to the eigenvectors and eigenvalues of $\mathbf{D}(\mathbf{x})$, respectively. The background color map indicates the magnitude $\text{Tr}[\mathbf{D}(\mathbf{x})]$, and white dots represent the observed data points. The axes display values mapped from \mathbf{x} back to the original variable space via linear fitting for visualization.

(right panel), the region of high inequality and high democracy is marked by low-magnitude drift vectors (darker colors), yet the streamlines show a consistent directional alignment toward the low-democracy trap. This implies that while high inequality may not trigger a rapid deterministic collapse in wealthy societies, it leads to a loss of structural resilience. In this regime, the restoring forces that typically sustain democracy effectively vanish, leaving the system structurally unanchored and weakly but consistently biased toward the low-democratic region.

Inferred diffusion fields $\mathbf{D}(\mathbf{x})$. The estimated diffusion field $\mathbf{D}(\mathbf{x})$ reveals a striking anisotropy in stochastic fluctuations. The diffusion ellipses are predominantly elongated along the democracy axis while remaining narrow along the inequality axis. This anisotropy highlights a disparity in fluctuation magnitudes: while economic inequality is characterized by low diffusivity, indicating robustness against random shocks, democracy scores exhibit significantly higher volatility.

Spatially, the diffusion magnitude reveals a dependency on economic development. As GDP/capita increases, the region of suppressed fluctuations noticeably narrows along the inequality axis. In high-GDP contexts (right panel), while low-inequality states remain within a low-noise regime (dark blue regions), markedly elevated fluctuation intensities emerge in the high-inequality region. Notably, this amplification is most pronounced in the intermediate zone separating high and low democracy (yellow regions). This implies that in wealthy societies with high inequality, the transition path between political regimes becomes highly volatile, contrasting with the quiescent stability of the low-inequality state.

Crucially, this amplification in the transition zone serves as a hallmark of critical transition or tipping

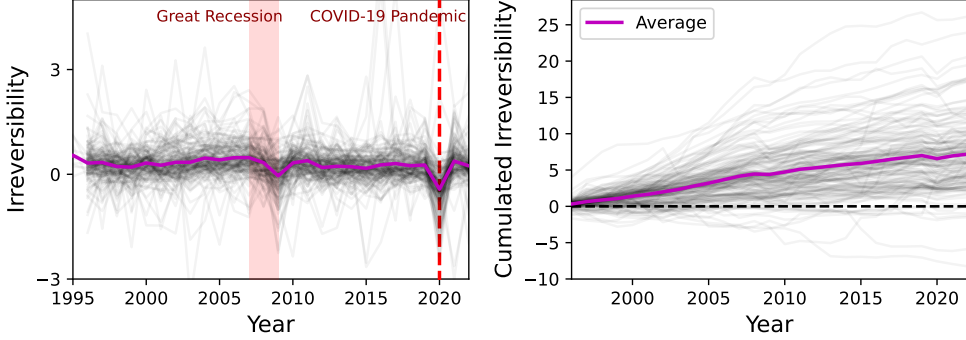


Figure 6: Evolution of Irreversibility and Cumulated Irreversibility (1995–2022). (Left) Annual irreversibility showing individual trajectories (grey) and their average (magenta). Notable dips correspond to the Great Recession (shaded area) and the COVID-19 pandemic (dashed line). (Right) Long-term upward trend in cumulated irreversibility, indicating a persistent accumulation of irreversible dynamics over the observed period.

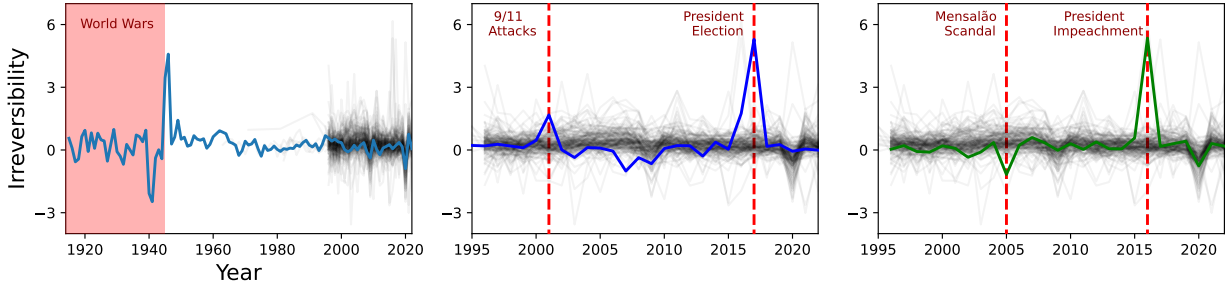


Figure 7: Impact of political shocks on irreversibility. Red shaded regions and dashed lines denote key political shocks. (Left) Century-scale view of France's irreversibility, including the impact of the World Wars. (Middle) Spikes in the U.S. trajectory associated with the 9/11 Attacks and the Presidential Election. (Right) Political crises in Brazil, highlighted by the Mensalão Scandal and the impeachment of the President. In all panels, colored lines represent the specific country's trajectory, while grey lines indicate the background ensemble of other trajectories for comparison.

point [51, 52]. Combining this with our drift analysis, where we identified a vanishing restoring force in this exact region, the physical picture becomes clear: high inequality erodes the deterministic resilience of the system. In this mechanically unanchored state, the amplified stochasticity becomes the dominant driver, actively destabilizing the system, and increasing the probability of a noise-induced transition toward the low-democracy trap.

5.3 Irreversibility

The irreversibility serves as a dynamical diagnostic that quantifies the alignment of a trajectory with the intrinsic probability current. Positive values indicate motion along the deterministic drift, whereas negative values suggest dynamics moving upstream against the prevailing flow. Figure 6 illustrates the evolution of irreversibility for the global political economy from 1995 to 2022. The cumulative irreversibility Σ (Right)

exhibits a persistent upward trend, confirming that the global system is continuously evolving away from equilibrium. However, the time-resolved irreversibility σ_t (Left) reveals that this directionality is strictly conditional; sharp dips correspond to major global crises such as the Great Recession (c. 2008) and the COVID-19 pandemic (2020). Physically, these drops indicate moments where trajectories deviate from the deterministic drift. During these periods, the system exhibits dynamics that are uncorrelated with or directly opposed to the intrinsic arrow of time, rather than following the structural trend.

This metric effectively identifies dynamical outliers. Countries exhibiting negative cumulative irreversibility in our sample, including *Burundi*, *Syria*, and *Yemen*, correspond to regions suffering from severe instability. Consistent with our definition, negative irreversibility implies that these trajectories are running counter to the inferred global dynamics. Their evolution is not governed by the typical laws of political economy observed in the ensemble, but instead characterizes a regime where the system consistently moves against the probabilistic tendency, creating a dynamical anomaly relative to the global structure.

At the national level, irreversibility provides a time-resolved detector of political shocks (Fig. 7). Distinct fluctuations in the irreversibility of *France*, *the United States*, and *Brazil* align with major historical episodes, ranging from wars to institutional crises, without requiring manual annotation. Crucially, unlike simple volatility measures, irreversibility distinguishes the dynamical nature of these events: it reveals whether a specific shock accelerates the system along its structural path or disrupts its directionality. Consequently, by observing whether the irreversibility spikes, drops to zero, or turns negative during these episodes, we can classify historical events not just by their size, but by their alignment with the underlying structural dynamics of the political economy.

5.4 Exogenous perturbation detection

To quantify the exogenous perturbations that are not captured by the intrinsic dynamics, we analyze the normalized surprisal \tilde{s}_t of observed transitions as defined in Eq. (10). While irreversibility characterizes the directional alignment with the structural trend, it does not account for how unexpected a specific transition is. By computing the tail probability of \tilde{s}_t , we can identify external shocks; a near-zero tail probability indicates a transition that is statistically highly improbable, signaling the presence of strong exogenous perturbations that override the system's intrinsic noise.

Figure 8 presents the annual tail probability for *France*, *the United States*, and *Brazil*. The results confirm that this metric reliably detects the major shocks identified in the irreversibility analysis, such as the World Wars, the 9/11 Attacks, and the Mensalão Scandal. In these cases, the events were both structurally impactful (high magnitude of irreversibility) and statistically extreme (low tail probability).

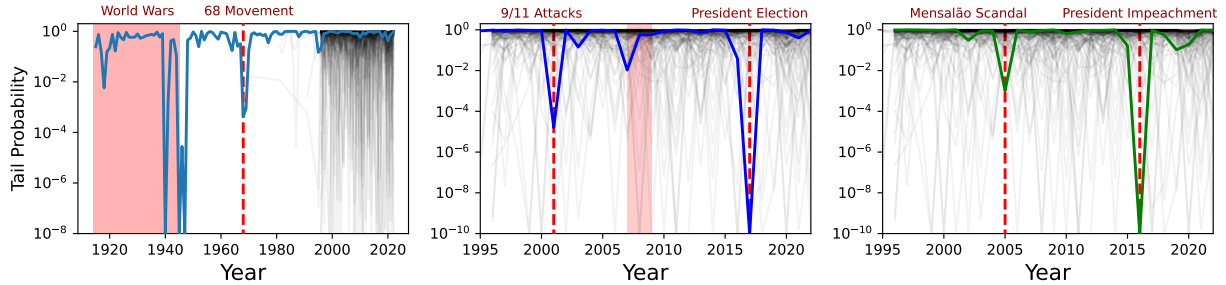


Figure 8: Tail probabilities indicating the likelihood of transition occurrences, serving as a proxy for exogenous perturbations. Red shaded regions and dashed lines denote key shocks. (Left) Century-scale view of France’s tail probability, including the impact of the World Wars and the 1968 movements. (Middle) Spikes in the U.S. trajectory associated with the 9/11 Attacks, the Great Recession, and the Presidential Election. (Right) Political crises in Brazil, highlighted by the Mensalão Scandal and the impeachment of the President. In all panels, colored lines represent the specific country’s trajectory, while grey lines indicate the background ensemble of other trajectories for comparison.

However, the tail probability reveals dynamical anomalies that irreversibility alone may overlook. A striking example is the trajectory of France (Left panel). While the World Wars appear as deep anomalies in both metrics, the civil unrest of May 1968 (“68 Movement” in Fig. 8) emerges as a distinct anomaly only in the tail probability analysis. Physically, this suggests a nuanced distinction in the nature of the event: the 1968 protests induced a statistically rare displacement (low tail probability), yet the transition itself did not instantaneously possess a directional bias against the intrinsic drift (low magnitude of irreversibility). This comparison demonstrates that the tail probability serves as a complementary diagnostic, enabling the detection of exogenous perturbations that violently shake the system regardless of their directional impact.

6 Application 2: Historical Civilizations

6.1 Construction of the state space

To evaluate the robustness of our framework in a data-sparse regime, we apply it to the *Polaris dataset* from the Seshat global history databank [16], which covers a diverse set of geographic regions across the globe, tracking polities that occupied these regions over long historical horizons. By systematically coding hundreds of sociopolitical variables, ranging from social stratification and governance to infrastructure, Seshat effectively transforms the vast, qualitative corpus of historical knowledge into a structured, quantitative format. From the *Polaris dataset*, we define the macroscopic state of a polity as a vector $\mathbf{x}_t \in \mathbb{R}^2$ spanned by two core indices: *Scale*, capturing the material magnitude of polities (population, territorial extent, urbanization), and *Computation*, capturing the capacity for information processing and control (bureaucratic organization, record-keeping, money system, infrastructure, and related features).

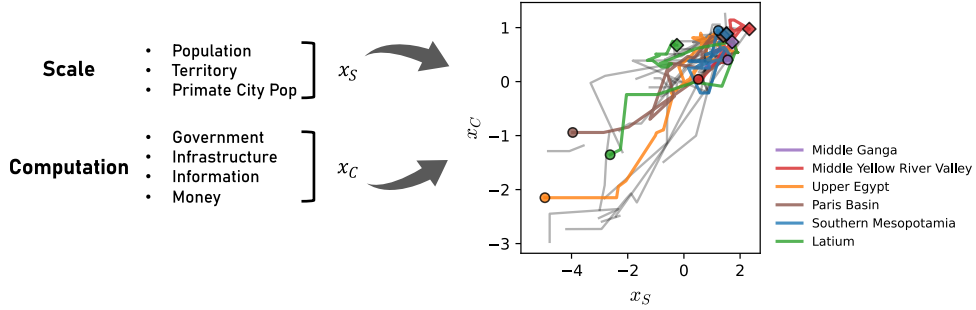


Figure 9: Trajectories of Natural Geographic Areas (NGAs) in the Scale-Computation plane. Colored paths trace the historical evolution of representative countries, illustrating diverse developmental patterns. The circle denotes the starting year, and the diamond indicates the most recent year. Grey lines depict the trajectories of other countries.

The resulting dataset consists of trajectories across 27 Natural Geographic Areas (NGAs), providing a unique opportunity to test dynamical theories (see Fig. 9). However, the data are extremely sparse; the baseline sampling interval is 100 years, and frequently exceeds this duration, yielding only ~ 250 region-period observations in total. Moreover, the measurements are inherently noisy. The coding of Polaris indices relies on expert historical judgment, where disagreements regarding categorization or timing introduce measurement errors distinct from the system’s intrinsic stochastic fluctuations.

To overcome these limitations, we employ the npSDE estimator (Sec. 4.2), particularly well suited to this sparse and irregularly sampled setup. By assuming that diverse regions share common drift $F(\mathbf{x})$ and diffusion $D(\mathbf{x})$ structures, this framework allows us to pool information across fragmented local histories to rigorously reconstruct the global landscape of civilizational evolution. Here, we utilize the raw physical observation intervals (i.e., $\alpha = 1$) but perform the forward simulation using a fine internal discretization step of $\delta t = 10^{-1}$ to accurately approximate the continuous-time evolution bridging the coarse data points.

6.2 Global dynamics of scale and computation

Figure 10 shows the inferred drift field for the Polaris state space. Each arrow indicates the local average direction of motion $\mathbf{F}(\mathbf{x})$, and color encodes the magnitude of the drift vector. Superimposed on this field (in later figures) are the empirical trajectories for individual regions.

Several regularities are immediately apparent. At low levels of Scale and Computation, the drift points broadly toward higher values of both indices: small, low-complexity polities are, on average, pulled toward greater population, territory, and information-processing capacity. As one moves into the intermediate range of the state space, the drift tends to flatten and bend, indicating a form of maturity plateau: further expansion in Scale is still possible, but the gains in Computation become more incremental. The estimated diffusion is moderate throughout most of the space, suggesting that very large jumps are possible but not typical.

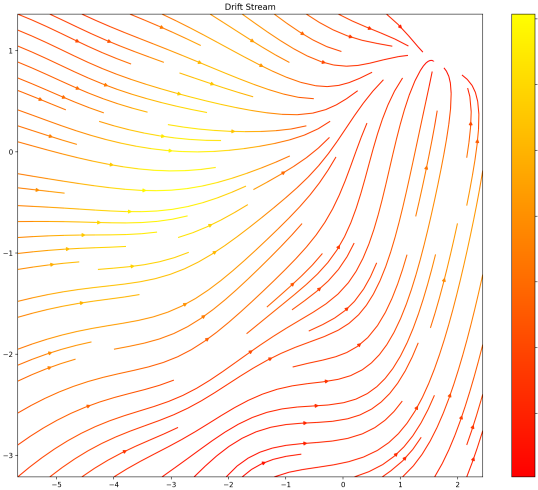


Figure 10: Inferred drift field on the Scale-Computation plane.

Overall, the global dynamics resemble a funnel: many trajectories originate near the bottom-left, and only a subset reach the upper-right, high-complexity region.

This global field provides the baseline against which we interpret individual historical episodes. The perturbation measure—the negative log transition density $-\log p(\mathbf{x}_{t+\Delta} | \mathbf{x}_t)$ —tells us when a polity takes a step that is unusually large or oddly directed relative to the drift and diffusion implied by Figure 10. The irreversibility score—the log-likelihood ratio between a forward step and its time-reversed counterpart, $\log p(\mathbf{x}_{t+\Delta} | \mathbf{x}_t) - \log p(\mathbf{x}_t | \mathbf{x}_{t+\Delta})$ —tells us whether such steps are effectively one-way or could easily be undone under the same dynamics. We now illustrate how these quantities behave for three instructive regions: the Paris Basin, Latium, and the Middle Yellow River Valley.

6.3 Paris Basin: a directional shift toward computational capacity

Figure 11 plots the Paris Basin trajectory in the Scale–Computation plane, together with the forward transition log density and the irreversibility score. The trajectory exhibits a long-run ascent in both dimensions: Scale rises early and persistently, while Computation increases more gradually, with a pronounced acceleration over a relatively short interval. In the language of the fitted SDE, much of the path follows the typical direction of motion implied by the global drift field: successive states move along the broad “funnel” direction toward higher Scale and higher Computation.

A salient feature of the Paris Basin series is a rapid rise in Computation that occurs while Scale continues to increase. This episode coincides with a clear dip in the forward transition log density, indicating that the model

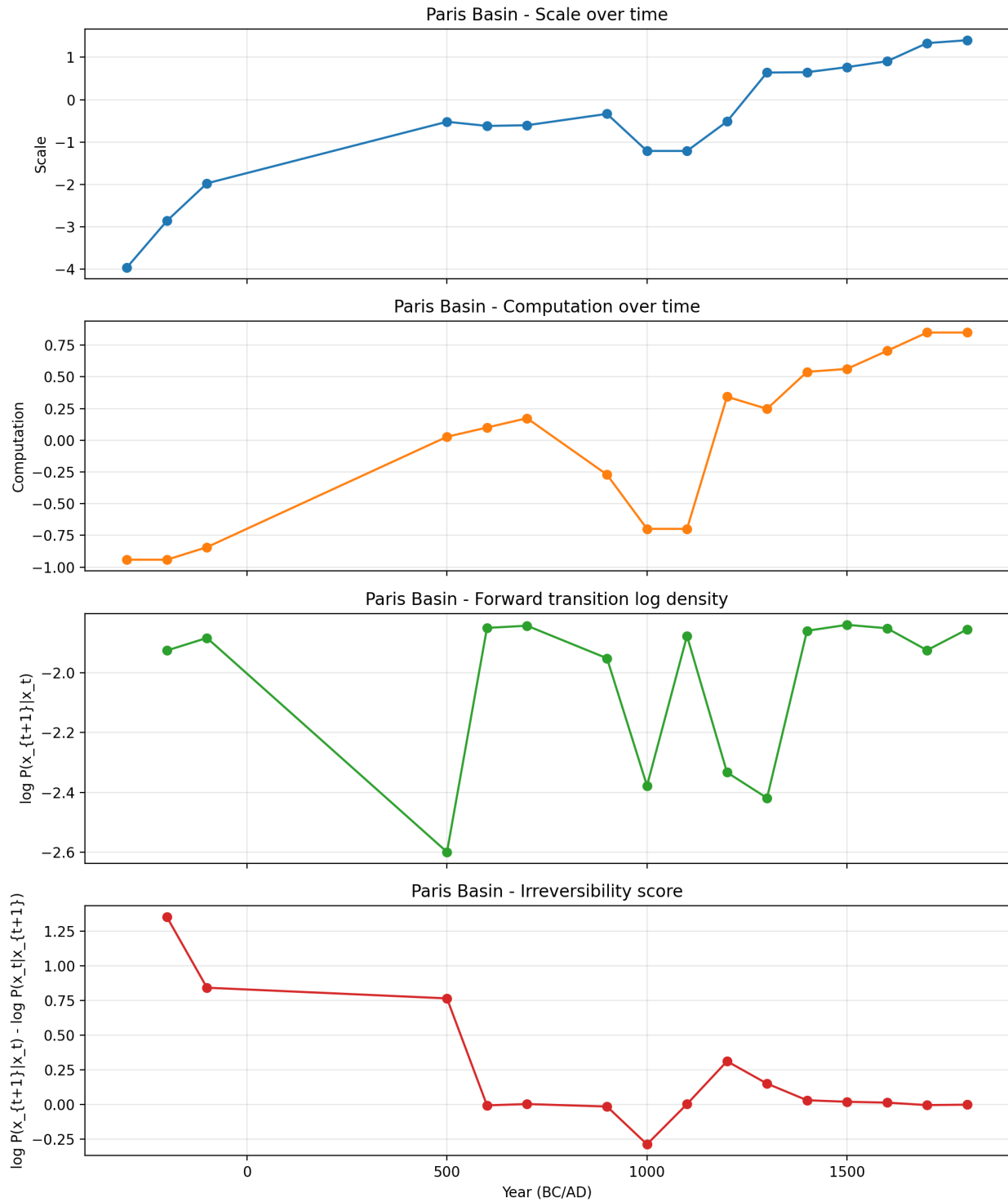


Figure 11: Paris Basin: trajectory in Scale and Computation, perturbation measure, and irreversibility score over time.

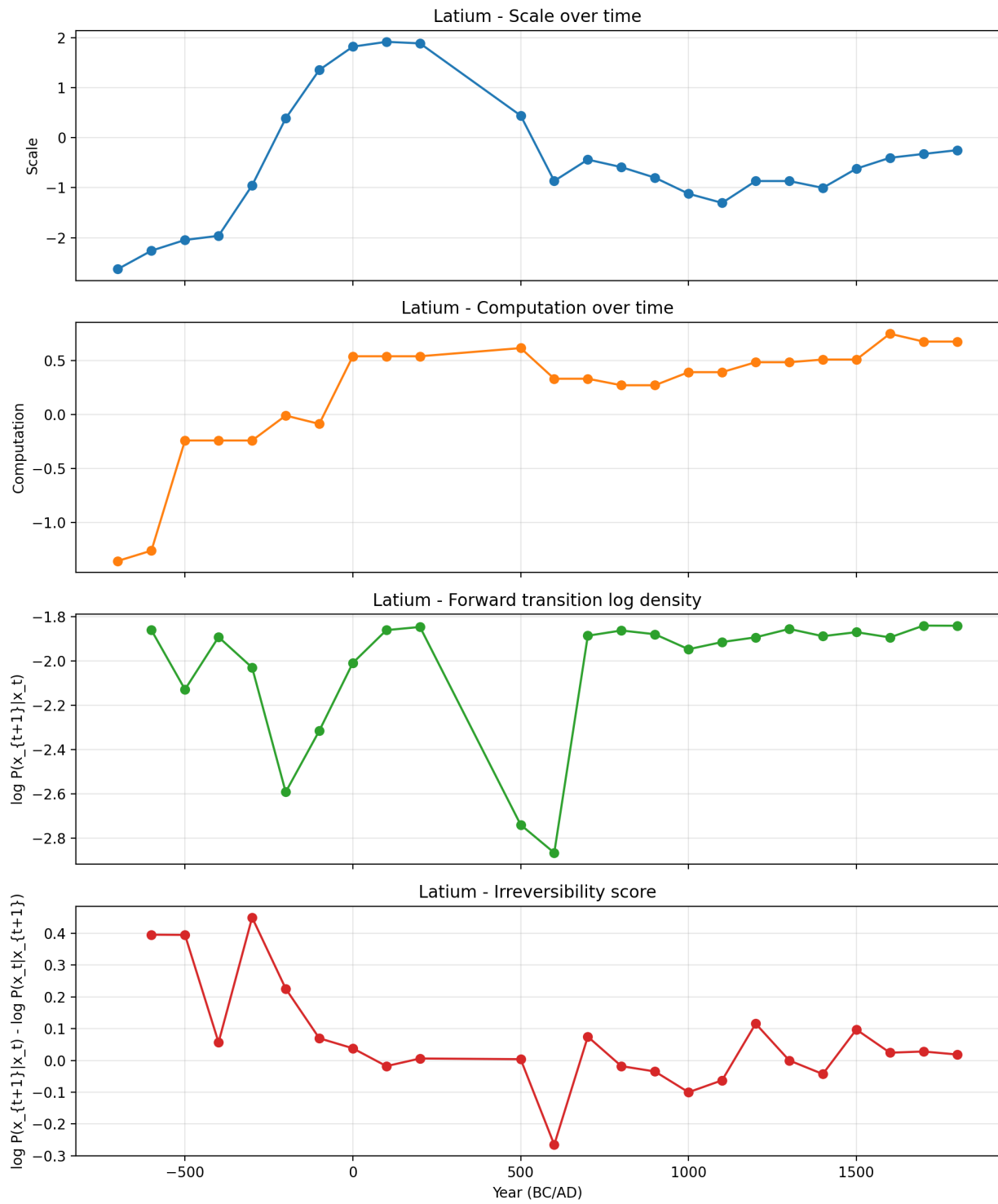


Figure 12: Latium: trajectory in Scale and Computation, perturbation measure, and irreversibility score over time.

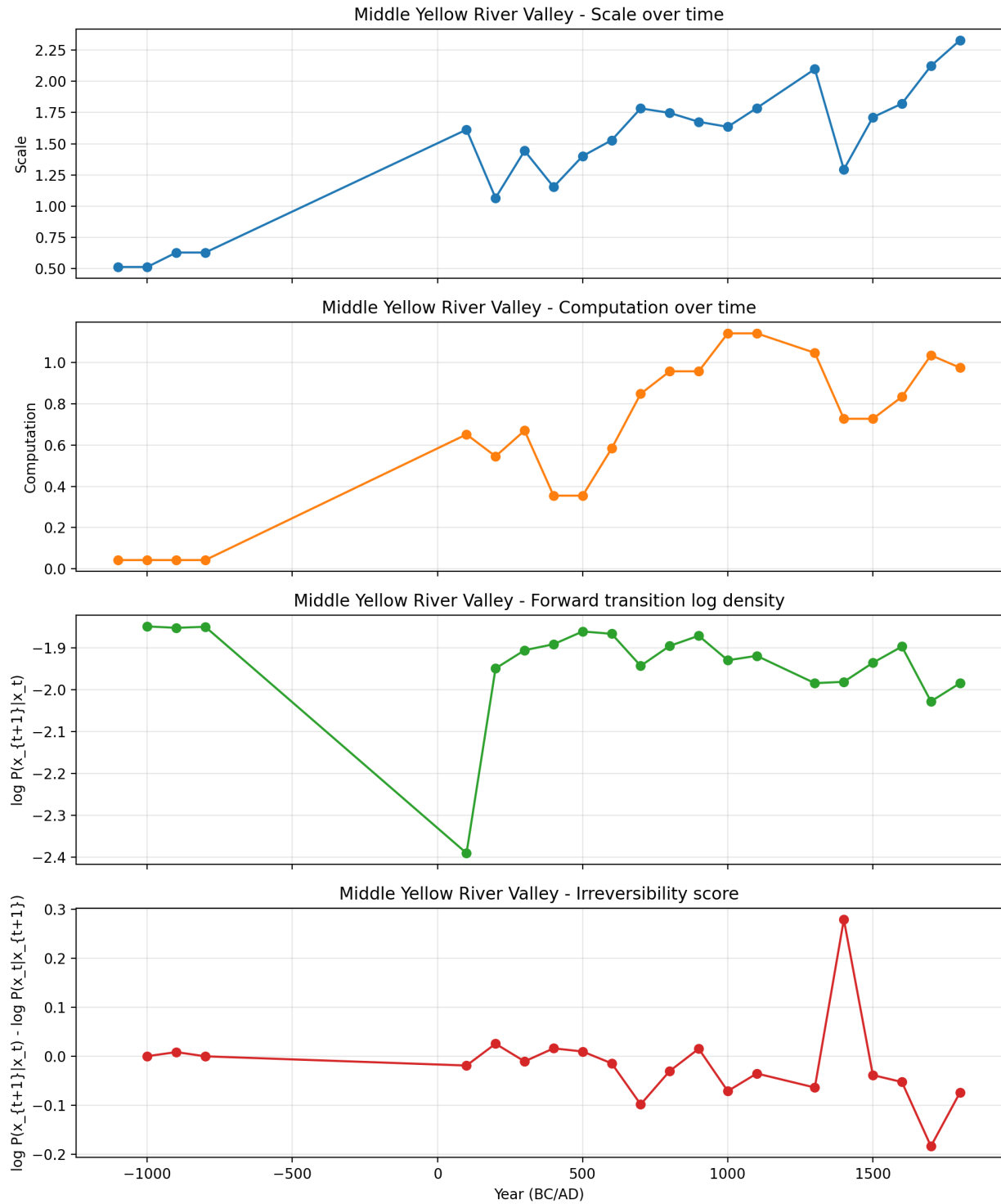


Figure 13: Middle Yellow River Valley: trajectory in Scale and Computation, perturbation measure, and irreversibility score over time.

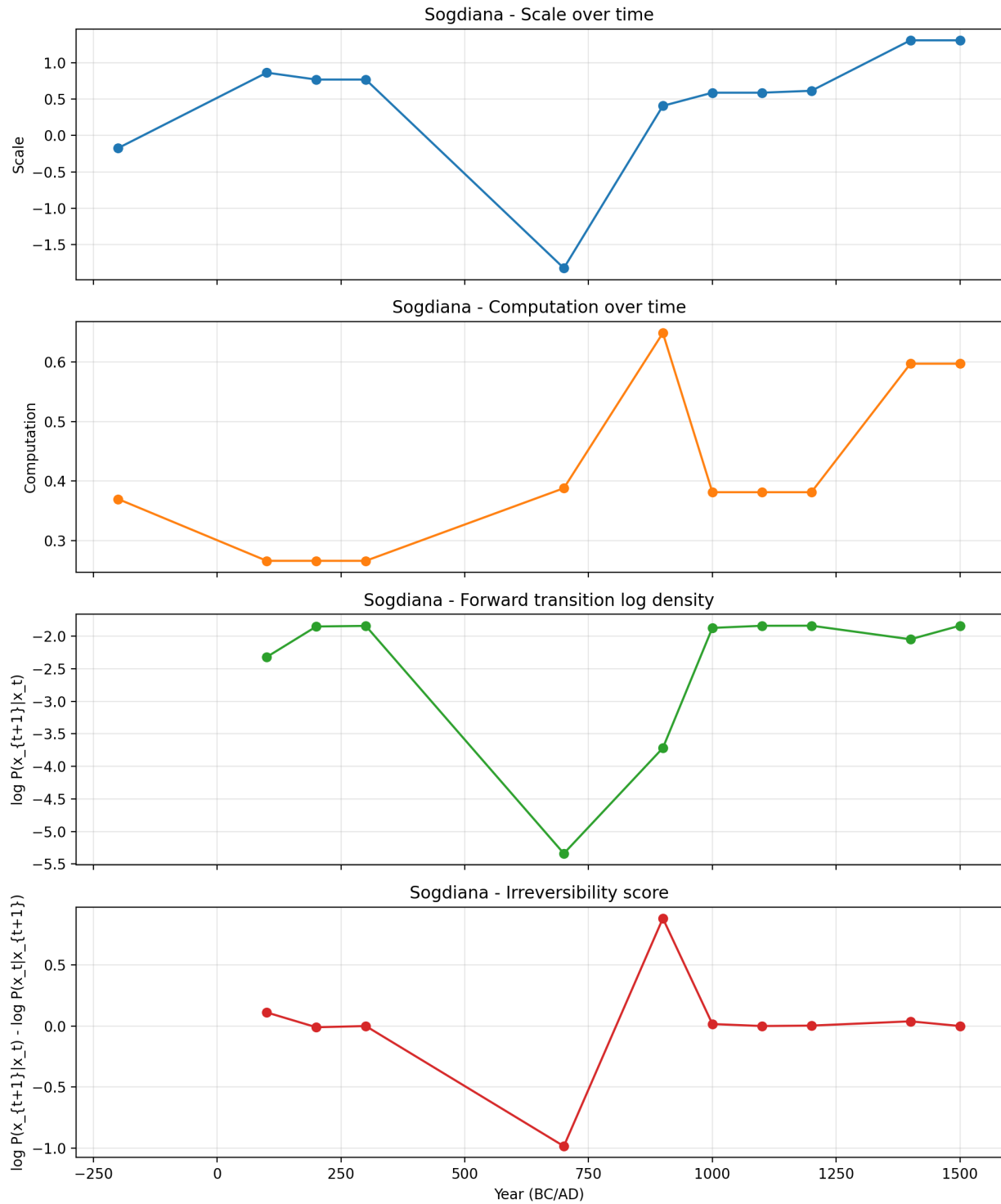


Figure 14: Sogdiana: trajectory in Scale and Computation, perturbation measure, and irreversibility score over time.

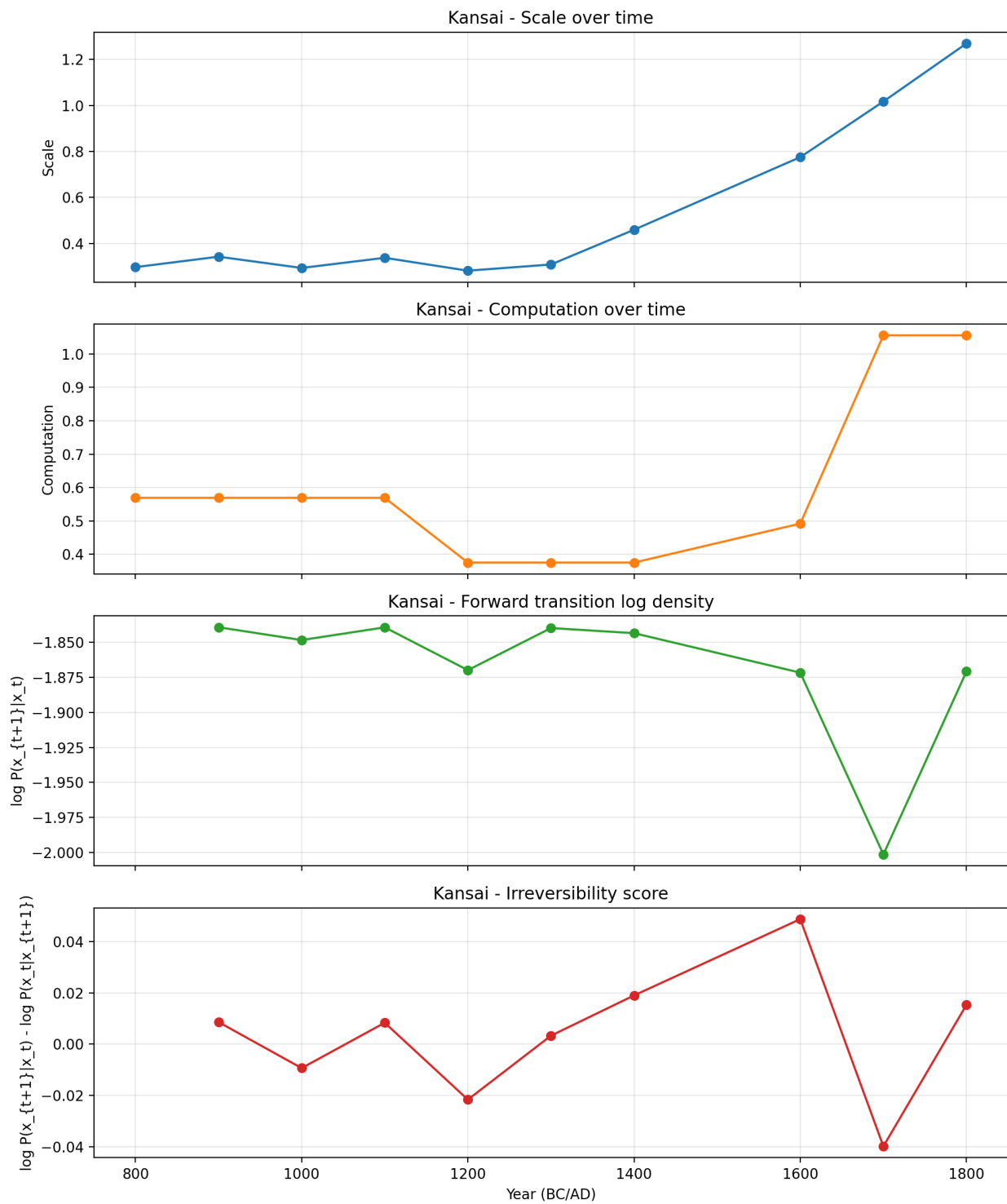


Figure 15: Kansai: trajectory in Scale and Computation, perturbation measure, and irreversibility score over time.

assigns relatively low probability to such a sharp acceleration in Computation given the immediately preceding state. Historically, a natural hypothesis is that this movement reflects a discrete transition in information-processing institutions rather than incremental demographic growth—for example, the consolidation of durable fiscal-administrative systems, the professionalization of bureaucracy, or the diffusion of record-keeping and legal infrastructure that raises effective state capacity. Importantly, our diagnostics do not identify *which* mechanism dominates; rather, they identify *when* the data imply a rapid reconfiguration that is atypical given the immediately preceding state, thereby prioritizing intervals for closer archival and historiographic scrutiny.

The irreversibility score around this transition is modest in magnitude relative to the most extreme cases in the sample, but informative in sign: when positive, it suggests that the movement is directionally structured rather than a symmetric fluctuation. One interpretation is that once administrative complexity crosses a threshold (e.g., the accumulation of codified procedures, routinized taxation, or bureaucratic specialization), reversal becomes less likely under the same dynamics, even if the initial jump is statistically surprising. Taken together, the Paris Basin illustrates a case where the stochastic dynamics highlight a specific interval as an unusually rapid *change in the composition of complexity* (toward Computation) and thus a promising target for historical investigation.

6.4 Latium: institutional takeoff versus imperial contraction

Latium provides a complementary contrast between growth episodes and contractions (Figure 12). The early part of the trajectory shows a rapid rise from low Scale and low Computation toward substantially higher values, consistent with an “institutional takeoff” that moves the region into a different part of the state space. Such an upward transition can be read as the emergence of durable coordination technologies: standing administrative structures, expanded fiscal extraction, infrastructural investments, and the institutionalization of command and control across larger territories. The corresponding dip in forward transition log density indicates that the move is statistically atypical given the prior state—consistent with a discontinuity in institutions rather than a smooth continuation of previous trends.

A second salient feature is a pronounced decline in Scale accompanied by a drop or flattening in Computation. This contraction aligns naturally with the historical arc of imperial fragmentation and the decline of Western Roman political integration. In the diagnostics, this episode coincides with the minimum of the forward transition log density in the Latium series, marking it as the most surprising Latium transition under the learned dynamics. The irreversibility score around the collapse is near zero or negative, suggesting that while the drop is abrupt and statistically unexpected given the preceding state, it is not intrinsically “one-way” under the global dynamics: movements toward lower-complexity configurations are

sufficiently common elsewhere that the reverse transition is not strongly disfavored. This distinction matters for interpretation. It is consistent with a view in which the fall represents a large exogenous or compound shock (e.g., political-military fragmentation, fiscal crisis, or cascading disruptions) rather than a deterministic drift toward an absorbing “collapse basin.”

These two moments illustrate the substantive value of separating perturbation from irreversibility. The model flags (i) an upward institutional transition that is directionally structured, and (ii) a later contraction that is an extreme surprise but not strongly irreversible. The former suggests the onset of a new regime of coordination; the latter suggests an event-like disruption whose causes require historical explanation beyond extrapolating local trends.

6.5 Middle Yellow River Valley: sustained drift with episodic contractions and periodization signals

The Middle Yellow River Valley (MYRV) exhibits sustained high Scale and rising Computation over the long run, punctuated by intermittent downturns (Figure 13). Relative to regions that undergo sharp state-space displacements, much of the MYRV trajectory lies close to the global drift direction: forward transition log densities are comparatively stable for extended periods, indicating that many transitions are statistically compatible with the cross-polity dynamics learned by the model.

Within this generally coherent trajectory, however, the diagnostics provide two kinds of guidance for historians. First, large step-like movements over long sampling gaps can yield low forward log density because the implied jump is large relative to local diffusion. These are precisely the intervals where historians would want to disaggregate whether the apparent “jump” reflects a genuine discontinuity in state formation or instead reflects measurement timing, interpolation, or heterogeneity in the underlying sources. Second, some contractions that jointly reduce Scale and Computation can produce elevated positive irreversibility even when the perturbation is not the most extreme in absolute magnitude, suggesting directionally structured downturns where reversals are less likely under the learned dynamics.

A particularly relevant interpretation for MYRV concerns periodization around major dynastic transitions. For example, historians often emphasize discontinuities in political integration and administrative reach around the late Yuan and early Ming periods, alongside possible definitional or coding ambiguities in the underlying historical record. In the state-space representation, any confusion or boundary misalignment between regimes—whether due to genuine rapid restructuring, changes in the unit of analysis, or shifts in source coverage—should manifest as a locally unexpected step (low forward log density), potentially coupled with distinctive irreversibility patterns if the transition reorganizes the state into a qualitatively different

configuration. The key point is not that the model “identifies” a dynasty *per se*, but that it identifies candidate intervals where periodization assumptions and coding decisions are most consequential and therefore merit closer expert adjudication.

6.6 Other regions and overall patterns: anomalies as prompts for targeted inquiry

Figures 14 and 15 illustrate further contrasts that clarify how these diagnostics can be used. Sogdiana (Figure 14) displays an extreme perturbation: the forward transition log density drops sharply during a steep contraction in Scale, indicating that the learned dynamics assign very low probability to such a rapid displacement from the prior state. Historically, Sogdiana sits at a crossroads of long-distance trade networks and imperial contestation, where abrupt reconfigurations can plausibly arise from external shocks (e.g., disruptions in trade corridors, conquest, or ecological stress) and from rapid reorganization of regional political structures. At the same time, the diagnostic itself does not privilege any single narrative. Its contribution is to isolate the contraction as an event-like episode that is difficult to explain by extrapolating local drift, thereby motivating targeted historical investigation (and, where possible, triangulation across independent data sources).

Kansai (Figure 15), by contrast, follows a smoother increase in Scale with relatively modest perturbations for much of its timeline. The principal standout is a discrete rise in Computation accompanied by a dip in forward transition log density. A plausible historical hypothesis is that this reflects rapid institutional innovation or consolidation of administrative technologies, rather than gradual accumulation—for example, shifts in governance capacity, legal-administrative standardization, or infrastructural and informational integration. Yet the irreversibility remains small in magnitude, suggesting that the change is statistically surprising but not structurally one-way under the learned dynamics: it resembles an atypical acceleration rather than an irreversible regime switch.

Taken together, these regional cases illustrate the intended use of the framework. The goal is not to replace historical explanation with a purely statistical narrative, but to provide *triage*: to identify intervals where the observed motion in the Scale–Computation space is locally unexpected (low transition log density) and/or directionally structured (high irreversibility). Some flagged episodes admit immediate historical interpretations (e.g., imperial contraction in Latium). Others may reflect coding boundaries, definitional shifts, or multi-causal transitions that are not easily reducible to a single event. In both cases, the diagnostics serve the same function: they guide historians toward periods where additional qualitative and source-critical work is likely to be most informative, and where competing narratives make sharply different predictions

about the direction and magnitude of institutional change.

7 Discussion

This paper proposes a stochastic differential equation (SDE) framework as a general language for inferring and analyzing the characteristics of historical and social trajectories. While we have shown empirical results that demonstrate the descriptive and diagnostic power of the SDE framework, its application to social science raises several points worthy of methodological, interpretive, and philosophical discussion. In this section, we discuss practical considerations and limitations that arise when fitting SDEs to social and historical data, the importance of choices in SDE inference, and the broader conceptual implications of treating social dynamics as intrinsically stochastic.

7.1 Limitations in data quality and dynamics identifications

A first and fundamental caveat concerns the quality and structure of social data itself. Compared to physical systems that are often controllable or reproducible, social systems are observed through sparse, noisy, and irregularly sampled historical records, frequently mediated by indirect indicators whose meanings and scales are not necessarily commensurable across time or contexts [20]. Even when the number of observed units is large, the temporal density of observations within each unit is often severely limited, observation periods rarely align across units, and missing values are pervasive. As in any fitting-based inference, such data limitations inevitably force some form of imputation or interpolation, which already weakens the direct correspondence between the fitted model and the underlying generative process.

Crucially, it is precisely these features of social data—short time series and coarse temporal resolution—that exacerbate a more fundamental limitation shared by all SDE-based inference: the identifiability of the dynamics themselves. When the sampling interval is fixed, drift and diffusion cannot be independently identified without bias; the diffusion term dominates the likelihood, while drift enters only at higher order, leading to systematic underestimation of drift and overestimation of diffusion [53, 54]. While this identifiability problem is intrinsic to SDE fitting in general, the sparse and irregular temporal structure of social data exacerbates it in social-scientific applications. In particular, this trade-off implies that apparent features of the inferred social dynamics, such as weak restoring forces or state-dependent volatility, may partly reflect data limitations rather than substantive social mechanisms.

Consequently, estimated drift terms should not be interpreted as direct measurements of causal forces, nor diffusion terms as mere residual noise. Instead, fitted SDEs are best understood as reduced-form dynamical representations that characterize local tendencies, variability, and stability of social processes. Within these

limits, SDE-based models remain valuable as diagnostic tools for probing irreversibility and sensitivity to perturbations, hence offering a coherent probabilistic framework for reasoning about uncertainty and path dependence in historical trajectories.

7.2 Homogeneity and independence assumptions

The problem of data limitation also leads to issues in implicit homogeneity assumptions in the method, namely, categorical and temporal homogeneity. Again, as with other fitting-based time series inferences, a set of data used to learn a single drift and diffusion field in SDE fitting naturally presupposes that that set of data originated from the same environment throughout all time periods of interest, without affecting influences on each other [55]. This could be bold and even incorrect assumptions when dealing with trajectories of interacting social entities (individuals, countries, etc.) of diverse characteristics over a long period [56]; for instance, one can argue that China and the Netherlands should not be assumed as sharing the same developmental surroundings, the rules of the capitalistic economy before the 1980s and after are fundamentally different and thus should be treated separately, nor that countries embedded in the globalized economy after the 1990s evolve independently of one another.

For the categorical homogeneity, one way to circumvent the issue is by splitting the collection of entities to be analyzed into socio-historically relevant subsets (or more systematically, clusters obtained from community detection methods of trajectory embeddings), performing separate fittings for each, and assuming categorical homogeneity holds within each subset. But this comes with a cost of further sparsifying the already scarce dataset, which inevitably worsens the quality and certainty of each fitting. One can also attempt to treat categories and time as separate variables and extend the state space, or adopting time-varying drift and diffusion field, but they yield a similar sparsification problem due to the increased state space dimension.

In practice, categorical and temporal heterogeneity cannot be fully resolved given the intrinsic limitations of historical and social data. Rather than treating these issues as technical flaws to be eliminated, they are better understood as modeling assumptions whose consequences must be made explicit. Pragmatically, robustness can be assessed by comparing results across alternative partitions of the data, evaluating generalization via cross-validation over entities or time blocks, and interpreting systematic increases in perturbation or irreversibility measures as potential signals of regime shifts or violations of the homogeneity assumption itself. From this perspective, SDE-based models are particularly advantageous in that they make such violations empirically visible through changes in local transition probabilities and path-wise likelihoods, rather than absorbing them silently into residual terms as in many static or purely regression-based approaches.

7.3 State space design and interpretability

Another noteworthy point for SDE fitting is the construction of the state space. The SDE framework favors a low-dimensional continuous state space that can represent the relevant historical dynamics, which is not an innocuous condition. The choice of variables and any dimensionality reduction applied to them implicitly encodes theoretical commitments about what aspects of social reality matter and on what timescales [19, 57].

Blindly including all available variables and applying unsupervised dimensionality reduction (e.g., PCA) can improve computational and analytical tractability, but may come at the cost of interpretability. Some variables may be endogenous summaries of others, while others may correspond to institutional or cultural features that change discontinuously or are poorly approximated as continuous processes. Variables that primarily reflect coding conventions, expert disagreement, or archival availability may be particularly problematic, as they can inflate diffusion estimates without corresponding to genuine social volatility.

In addition, data types admissible within the SDE framework are also limited by its construction as well. SDEs assume that each state variable evolves in a continuous, typically unbounded numerical space. In contrast, much of the data available in social science is categorical or ordinal, or consists of continuous variables constrained to bounded ranges. Mapping such heterogeneous data into a continuous state space (often through encoding schemes, normalization, or dimensionality reduction) requires additional modeling choices that are rarely neutral. These transformations implicitly smooth, interpolate, or metrize social categories in ways that may lack a clear substantive interpretation, further reinforcing theoretical assumptions about continuity, comparability, and the scales at which social change is presumed to occur.

For these reasons, state space construction should be guided by theory as well as data availability. SDEs are best suited to variables that plausibly evolve continuously and exhibit local dependence on their current state. When such assumptions are questionable, the resulting dynamics should be interpreted with caution, or alternative representations (e.g., regime-switching or hybrid models) should be considered. Ultimately, rather than treating dimensionality reduction as a separate preprocessing step, future studies should aim to develop a unified methodological framework that systematically integrates dimension reduction with SDE fitting in a manner tailored to the data conditions.

7.4 Relative advantages of SDE fitting methodologies

Among SDE models, an important methodological choice in applying such models to socio-historical data concerns how the drift and diffusion are inferred from observations. In this paper, we employ two complementary approaches: a neural-network-based formulation in the form of Langevin Bayesian Networks (LBN) and a nonparametric Gaussian-process-based SDE estimator (npSDE). Although both aim to recover effective

stochastic dynamics, they differ in their inductive biases, statistical objectives, and interpretations of what it means to “infer” an SDE from data [14, 15].

The Gaussian-process-based approach (e.g., npSDE) treats drift and diffusion as smooth latent functions over state space, equipped with explicit priors that enforce locality and regularity. This makes it particularly suitable for settings with sparse, irregularly sampled data and low-dimensional state spaces, where interpretability and uncertainty quantification of the inferred vector fields are central. In this regime, the GP prior acts as a strong but transparent regularizer, yielding a population-level description of effective dynamics. By contrast, the neural-network-based LBN approach adopts a more direct statistical stance. Rather than representing drift and diffusion as explicit latent functions with smoothness priors, the LBN formulation parameterizes the conditional transition distribution itself using a flexible function approximator, while retaining an SDE interpretation. This shift emphasizes predictive fidelity and scalability: given sufficient data, neural networks can capture highly nonlinear, anisotropic, and state-dependent dynamics that would be difficult to represent with kernel-based methods, at the cost of weaker interpretability and greater reliance on data availability and regularization choices.

These differences imply that the two approaches address distinct epistemic goals. GP-based SDE inference is best understood as characterizing structured, interpretable effective dynamics under strong smoothness assumptions, whereas neural-network-based methods aim to approximate empirical transition laws with minimal structural constraints. Accordingly, methodological choice should be treated as an empirical decision conditioned on data structure and research objectives. In this paper, we view the joint use of both approaches as complementary rather than redundant, helping to clarify which features of the inferred dynamics are robust to modeling assumptions. We note that further quantitative comparison among different methodologies is also possible, with measures such as negative loss likelihood for the unseen test dataset.

7.5 Interpretation of Statistical regularities and Causal mechanisms

A central interpretative question concerns how the estimated drift and diffusion terms should be understood in social contexts, and in particular whether they can be regarded as indicators of causal mechanisms. Unlike in many physical systems, these quantities cannot be straightforwardly identified with causal “forces” or intrinsic noise sources. Rather, they summarize conditional statistical tendencies: how systems with similar current states tend to change, on average and in variance, over the next observational interval. From the perspective of causal inference, such quantities correspond to associational regularities rather than interventional effects, and therefore cannot by themselves support strong causal claims [58]. This limitation also cautions against interpreting qualitative regularities uncovered by SDE fitting as guarantees about future dynamics under

altered institutional or historical conditions.

This does not imply, however, that SDE models are merely descriptive or explanatorily vacuous. By localizing trends and variability in state space, they can highlight regimes of stability, sensitivity, or unusually large fluctuations. Such patterns can generate testable hypotheses about underlying mechanisms, institutional constraints, or omitted variables. In this sense, SDE fitting complements causal and structural approaches by organizing complex temporal data into a coherent probabilistic framework that delineates what kinds of trajectories are typical, unstable, or exceptional. This pattern-oriented role aligns with a broader perspective from complexity science, in which statistical and stochastic models are valued not for recovering exact micro-level mechanisms, but for constraining the space of plausible dynamics and guiding subsequent mechanistic inquiry [59]. Nevertheless, we note that SDE inference alone cannot distinguish causal mechanisms from correlated regularities. Its primary contribution lies in organizing complex temporal data into a coherent probabilistic structure that can guide further theoretical and empirical investigation.

7.6 The meaning of stochastic explanation in social science

Finally, adopting an SDE perspective on social trajectories carries broad philosophical implications. Treating social dynamics as stochastic does not merely amount to adding noise to otherwise deterministic models, despite the mathematical appearance of stochastic terms. Rather, it asserts that uncertainty and variability are constitutive features of historical processes, not some observational residuals to be eliminated. This view directly challenges strong notions of historical determinism and historical inevitability, which assume that large-scale social trajectories unfold according to fixed and discoverable laws [60].

If diffusion terms are interpreted as capturing irreducible contingency, which arises from aggregated individual actions, unobserved interactions, or genuinely unpredictable events, then history is better understood not as a single realizable path, but as a distribution over possible trajectories. Here, the concept of agency and responsibility is reframed, as actions now shape probabilities and tendencies, rather than guaranteeing a single outcome. This probabilistic conception aligns with philosophical accounts that regard chance as an intrinsic and socially meaningful component of explanation [61], rather than a proxy for ignorance.

From this perspective, stochastic process models provide a formal language for navigating between structural constraints and contingency. Perturbation and irreversibility analysis from SDE fittings allow us to quantify when history appears tightly channeled by existing structures, when it is dominated by random fluctuations, and when singular events push systems onto qualitatively new paths. In doing so, they offer a bridge between quantitative modeling and long-standing debates in historical and social theory about chance, necessity, and agency.

7.7 Outlook

Looking ahead, we envision SDE-based approaches as both complementary and a well-theoretically grounded layer in the methodological toolkit of social and historical analysis. SDE models provide a disciplined way to interrogate trajectories, quantify uncertainty, and locate the boundaries between structural regularities and contingency. As richer longitudinal data and more flexible inference methods become available, this perspective may help integrate quantitative modeling with substantive theory, enabling a more nuanced understanding of how social systems evolve under uncertainty.

Acknowledgments

The authors thank Peter Turchin and Matilda Peruzzo for sharing the Polaris dataset from the Seshat databank. Y.B. was supported by the Global-LAMP Program of the National Research Foundation of Korea (NRF) grant funded by the Ministry of Education (No. RS-2023-00301976).

References

- [1] Karl Marx. *The Eighteenth Brumaire of Louis Bonaparte*. New York: Die Revolution, 1852.
- [2] Douglass C. North. *Institutions, Institutional Change and Economic Performance*. Cambridge: Cambridge University Press, 1990.
- [3] Paul A. David. “Clio and the Economics of QWERTY”. In: *The American Economic Review* 75.2 (1985), pp. 332–337.
- [4] Douglass C. North and Lance E. Davis. “Institutional Change and American Economic Growth: A First Step Towards a Theory of Institutional Innovation”. In: *The Journal of Economic History* 31.1 (1971), pp. 131–149.
- [5] Joshua D. Angrist and Jörn-Steffen Pischke. “The Credibility Revolution in Empirical Economics: How Better Research Design is Taking the Con out of Econometrics”. In: *Journal of Economic Perspectives* 24.2 (2010), pp. 3–30.
- [6] Peter Turchin. *Historical Dynamics: Why States Rise and Fall*. Princeton University Press, 2003. URL: <http://www.jstor.org/stable/j.ctt1wf4d45> (visited on 12/18/2025).
- [7] Peter Turchin. “Arise ‘Cliodynamics’”. In: *Nature* 454.7200 (2008), pp. 34–35.

[8] David H. Wolpert, Michael H. Price, Stefani A. Crabtree, Timothy A. Kohler, Jürgen Jost, et al. “The Past as a Stochastic Process”. In: *Journal of Computer Applications in Archaeology* 7.1 (2024). Position Paper, pp. 134–152. DOI: [10.5334/jcaa.113](https://doi.org/10.5334/jcaa.113). URL: <https://journal.caa-international.org/articles/10.5334/jcaa.113>.

[9] Simon Kuznets. “Economic growth and income inequality”. In: *Am. Econ. Rev* 45.1 (1955), pp. 1–28.

[10] Daron Acemoglu and James A Robinson. “Why did the West extend the franchise? Democracy, inequality, and growth in historical perspective”. In: *The quarterly journal of economics* 115.4 (2000), pp. 1167–1199.

[11] Armen Der Kiureghian and Ove Ditlevsen. “Aleatory or epistemic? Does it matter?” In: *Structural Safety* 31.2 (2009), pp. 105–112. DOI: [10.1016/j.strusafe.2008.06.020](https://doi.org/10.1016/j.strusafe.2008.06.020).

[12] Eyke Hüllermeier and Willem Waegeman. “Aleatoric and epistemic uncertainty in machine learning: An introduction to concepts and methods”. In: *Machine Learning* 110.3 (2021), pp. 457–506. DOI: [10.1007/s10994-021-05946-3](https://doi.org/10.1007/s10994-021-05946-3).

[13] Walter Scheidel. *The Great Leveler: Violence and the History of Inequality from the Stone Age to the Twenty-First Century*. Princeton University Press, 2017.

[14] Youngkyoung Bae, Seungwoong Ha, and Hawoong Jeong. “Inferring the Langevin equation with uncertainty via Bayesian neural networks”. In: *Chaos, Solitons & Fractals* 197 (2025), p. 116440. ISSN: 0960-0779. DOI: <https://doi.org/10.1016/j.chaos.2025.116440>. URL: <https://www.sciencedirect.com/science/article/pii/S0960077925004539>.

[15] Cagatay Yildiz, Markus Heinonen, Jukka Intosalmi, Henrik Mannerstrom, and Harri Lahdesmaki. “Learning stochastic differential equations with gaussian processes without gradient matching”. In: *2018 IEEE 28th International Workshop on Machine Learning for Signal Processing (MLSP)*. 2018, pp. 1–6. DOI: [10.1109/MLSP.2018.8516991](https://doi.org/10.1109/MLSP.2018.8516991).

[16] Peter Turchin, Rob Brennan, Thomas E. Currie, Kevin Feeney, Pieter François, et al. “Seshat: The Global History Databank”. In: *Cliodynamics* 6.1 (2015), pp. 77–107. DOI: [10.21237/C7clio6127917](https://doi.org/10.21237/C7clio6127917). URL: <https://doi.org/10.21237/C7clio6127917>.

[17] Jeffrey R. Edwards and Richard P. Bagozzi. “On the nature and direction of relationships between constructs and measures.” In: *Psychological Methods* 5.2 (2000), pp. 155–174. DOI: [10.1037/1082-989X.5.2.155](https://doi.org/10.1037/1082-989X.5.2.155). URL: <https://doi.org/10.1037/1082-989X.5.2.155>.

[18] Shawn Treier and Simon Jackman. “Democracy as a Latent Variable”. In: *American Journal of Political Science* 52.1 (2008), pp. 201–217. DOI: <https://doi.org/10.1111/j.1540-5907.2007.00308.x>. eprint: <https://onlinelibrary.wiley.com/doi/pdf/10.1111/j.1540-5907.2007.00308.x>. URL: <https://onlinelibrary.wiley.com/doi/abs/10.1111/j.1540-5907.2007.00308.x>.

[19] James Durbin and Siem Jan Koopman. *Time Series Analysis by State Space Methods*. Oxford University Press, May 2012. ISBN: 9780199641178. DOI: [10.1093/acprof:oso/9780199641178.001.0001](https://doi.org/10.1093/acprof:oso/9780199641178.001.0001). URL: <https://doi.org/10.1093/acprof:oso/9780199641178.001.0001>.

[20] Hubert M. Blalock, ed. *Measurement in the Social Sciences: Theories and Strategies*. Chicago: Aldine Publishing Company, 1974.

[21] Robert Zwanzig. *Nonequilibrium statistical mechanics*. Oxford University Press, 2001.

[22] Crispin William Gardiner. *Handbook of Stochastic Methods*. Springer Berlin, Heidelberg, 2004.

[23] Peter Turchin, Thomas E. Currie, Harvey Whitehouse, Pieter François, Kevin Feeney, et al. “Quantitative historical analysis uncovers a single dimension of complexity that structures global variation in human social organization”. In: *Proceedings of the National Academy of Sciences* 115.2 (2018), E144–E151. DOI: [10.1073/pnas.1708800115](https://doi.org/10.1073/pnas.1708800115). eprint: <https://www.pnas.org/doi/pdf/10.1073/pnas.1708800115>. URL: <https://www.pnas.org/doi/abs/10.1073/pnas.1708800115>.

[24] Jaeweon Shin, Michael Holton Price, David H. Wolpert, Hajime Shimao, Brendan Tracey, et al. “Scale and information-processing thresholds in Holocene social evolution”. In: *Nature Communications* 11.1 (May 2020), p. 2394. ISSN: 2041-1723. DOI: [10.1038/s41467-020-16035-9](https://doi.org/10.1038/s41467-020-16035-9). URL: <https://doi.org/10.1038/s41467-020-16035-9>.

[25] Hannes Risken. *Fokker-planck equation*. Springer, Berlin, 1996.

[26] Rudolf Friedrich, Joachim Peinke, Muhammad Sahimi, and M. Reza Rahimi Tabar. “Approaching complexity by stochastic methods: From biological systems to turbulence”. In: *Phys. Rep.* 506.5 (2011), pp. 87–162. ISSN: 0370-1573. DOI: <https://doi.org/10.1016/j.physrep.2011.05.003>. URL: <https://www.sciencedirect.com/science/article/pii/S0370157311001530>.

[27] Ignacio A. Martínez, Gili Bisker, Jordan M. Horowitz, and Juan M. R. Parrondo. “Inferring broken detailed balance in the absence of observable currents”. In: *Nature Communications* 10.1 (Aug. 2019), p. 3542. ISSN: 2041-1723. DOI: [10.1038/s41467-019-11051-w](https://doi.org/10.1038/s41467-019-11051-w). URL: <https://doi.org/10.1038/s41467-019-11051-w>.

[28] Fischer Black and Myron Scholes. “The Pricing of Options and Corporate Liabilities”. In: *Journal of Political Economy* 81.3 (1973), pp. 637–654. ISSN: 00223808, 1537534X. URL: <http://www.jstor.org/stable/1831029> (visited on 01/22/2026).

[29] Udo Seifert. “Stochastic thermodynamics, fluctuation theorems and molecular machines”. In: *Reports on Progress in Physics* 75.12 (Nov. 2012), p. 126001. DOI: [10.1088/0034-4885/75/12/126001](https://doi.org/10.1088/0034-4885/75/12/126001). URL: <https://doi.org/10.1088/0034-4885/75/12/126001>.

[30] Udo Seifert. “Entropy Production along a Stochastic Trajectory and an Integral Fluctuation Theorem”. In: *Phys. Rev. Lett.* 95 (4 July 2005), p. 040602. DOI: [10.1103/PhysRevLett.95.040602](https://doi.org/10.1103/PhysRevLett.95.040602). URL: <https://link.aps.org/doi/10.1103/PhysRevLett.95.040602>.

[31] J M R Parrondo, C Van den Broeck, and R Kawai. “Entropy production and the arrow of time”. In: *New Journal of Physics* 11.7 (July 2009), p. 073008. DOI: [10.1088/1367-2630/11/7/073008](https://doi.org/10.1088/1367-2630/11/7/073008). URL: <https://doi.org/10.1088/1367-2630/11/7/073008>.

[32] Dominic J. Skinner and Jörn Dunkel. “Improved bounds on entropy production in living systems”. In: *Proceedings of the National Academy of Sciences* 118.18 (2021), e2024300118. DOI: [10.1073/pnas.2024300118](https://doi.org/10.1073/pnas.2024300118). eprint: <https://www.pnas.org/doi/pdf/10.1073/pnas.2024300118>. URL: <https://www.pnas.org/doi/abs/10.1073/pnas.2024300118>.

[33] Christopher W. Lynn, Eli J. Cornblath, Lia Papadopoulos, Maxwell A. Bertolero, and Danielle S. Bassett. “Broken detailed balance and entropy production in the human brain”. In: *Proceedings of the National Academy of Sciences* 118.47 (2021), e2109889118. DOI: [10.1073/pnas.2109889118](https://doi.org/10.1073/pnas.2109889118). eprint: <https://www.pnas.org/doi/pdf/10.1073/pnas.2109889118>. URL: <https://www.pnas.org/doi/abs/10.1073/pnas.2109889118>.

[34] I. Di Terlizzi, M. Gironella, D. Herraez-Aguilar, T. Betz, F. Monroy, et al. “Variance sum rule for entropy production”. In: *Science* 383.6686 (2024), pp. 971–976. DOI: [10.1126/science.adh1823](https://doi.org/10.1126/science.adh1823). eprint: <https://www.science.org/doi/pdf/10.1126/science.adh1823>. URL: <https://www.science.org/doi/abs/10.1126/science.adh1823>.

[35] Thomas M. Cover and Joy A. Thomas. *Elements of Information Theory (Wiley Series in Telecommunications and Signal Processing)*. Wiley-Interscience, New York, 2006. ISBN: 0471241954.

[36] Nathanael Hoze, Deepak Nair, Eric Hosy, Christian Sieben, Suliana Manley, et al. “Heterogeneity of AMPA receptor trafficking and molecular interactions revealed by superresolution analysis of live cell imaging”. In: *Proc. Natl. Acad. Sci. U.S.A.* 109.42 (2012), pp. 17052–17057. DOI: [10.1073/pnas.1204589109](https://doi.org/10.1073/pnas.1204589109). URL: <https://www.pnas.org/doi/abs/10.1073/pnas.1204589109>.

[37] Mohamed El Beheiry, Maxime Dahan, and Jean-Baptiste Masson. “InferenceMAP: mapping of single-molecule dynamics with Bayesian inference”. In: *Nat. Methods* 12.7 (July 2015), pp. 594–595. ISSN: 1548-7105. DOI: [10.1038/nmeth.3441](https://doi.org/10.1038/nmeth.3441). URL: <https://doi.org/10.1038/nmeth.3441>.

[38] Titiwat Sungkaworn, Marie-Lise Jobin, Krzysztof Burnecki, Aleksander Weron, Martin J. Lohse, et al. “Single-molecule imaging reveals receptor–G protein interactions at cell surface hot spots”. In: *Nature* 550.7677 (Oct. 2017), pp. 543–547. ISSN: 1476-4687. DOI: [10.1038/nature24264](https://doi.org/10.1038/nature24264). URL: <https://doi.org/10.1038/nature24264>.

[39] Anna Frishman and Pierre Ronceray. “Learning Force Fields from Stochastic Trajectories”. In: *Phys. Rev. X* 10 (2 Apr. 2020), p. 021009. DOI: [10.1103/PhysRevX.10.021009](https://doi.org/10.1103/PhysRevX.10.021009).

[40] David B. Brückner, Pierre Ronceray, and Chase P. Broedersz. “Inferring the Dynamics of Underdamped Stochastic Systems”. In: *Phys. Rev. Lett.* 125 (5 July 2020), p. 058103. DOI: [10.1103/PhysRevLett.125.058103](https://doi.org/10.1103/PhysRevLett.125.058103). URL: <https://link.aps.org/doi/10.1103/PhysRevLett.125.058103>.

[41] Andonis Gerardos and Pierre Ronceray. “Principled Model Selection for Stochastic Dynamics”. In: *Phys. Rev. Lett.* 135 (16 Oct. 2025), p. 167401. DOI: [10.1103/1tdt-hvh7](https://doi.org/10.1103/1tdt-hvh7). URL: <https://link.aps.org/doi/10.1103/1tdt-hvh7>.

[42] David Lamouroux and Klaus Lehnertz. “Kernel-based regression of drift and diffusion coefficients of stochastic processes”. In: *Phys. Lett. A* 373.39 (2009), pp. 3507–3512. ISSN: 0375-9601. DOI: <https://doi.org/10.1016/j.physleta.2009.07.073>. URL: <https://www.sciencedirect.com/science/article/pii/S037596010900944X>.

[43] Xuechen Li, Ting-Kam Leonard Wong, Ricky T. Q. Chen, and David Duvenaud. “Scalable Gradients for Stochastic Differential Equations”. In: *Proceedings of the Twenty Third International Conference on Artificial Intelligence and Statistics*. Ed. by Silvia Chiappa and Roberto Calandra. Vol. 108. Proceedings of Machine Learning Research. PMLR, 26–28 Aug 2020, pp. 3870–3882. URL: <https://proceedings.mlr.press/v108/li20i.html>.

[44] Mozes Jacobs, Bingni W Brunton, Steven L Brunton, J Nathan Kutz, and Ryan V Raut. “Hypersindy: Deep generative modeling of nonlinear stochastic governing equations”. In: *arXiv preprint arXiv:2310.04832* (2023).

[45] Ting-Ting Gao, Baruch Barzel, and Gang Yan. “Learning interpretable dynamics of stochastic complex systems from experimental data”. In: *Nat. Commun.* 15.1 (July 2024), p. 6029. ISSN: 2041-1723. DOI: [10.1038/s41467-024-50378-x](https://doi.org/10.1038/s41467-024-50378-x). URL: <https://doi.org/10.1038/s41467-024-50378-x>.

[46] Wesley J Maddox, Pavel Izmailov, Timur Garipov, Dmitry P Vetrov, and Andrew Gordon Wilson. “A Simple Baseline for Bayesian Uncertainty in Deep Learning”. In: *Advances in Neural Information Processing Systems*. Ed. by H. Wallach, H. Larochelle, A. Beygelzimer, F. d’Alché-Buc, E. Fox, et al. Vol. 32. Curran Associates, Inc., 2019. URL: https://proceedings.neurips.cc/paper_files/paper/2019/file/118921efba23fc329e6560b27861f0c2-Paper.pdf.

[47] Michael Coppedge, John Gerring, Carl Henrik Knutsen, Staffan I. Lindberg, Jan Teorell, et al. *V-Dem [Country-Year/Country-Date] Dataset v15*. Varieties of Democracy (V-Dem) Project. Accessed via <https://v-dem.net>. 2025. DOI: [10.23696/vdemds25](https://doi.org/10.23696/vdemds25). URL: <https://doi.org/10.23696/vdemds25>.

[48] Facundo Alvaredo, Lucas Chancel, Thomas Piketty, Emmanuel Saez, and Gabriel Zucman. *World Inequality Database (WID.world)*. Accessed via <https://wid.world>. 2025. URL: <https://wid.world>.

[49] Jutta Bolt and Jan Luiten van Zanden. “Maddison-style estimates of the evolution of the world economy: A new 2023 update”. In: *Journal of Economic Surveys* 39.2 (2024), pp. 631–671. DOI: [10.1111/joes.12618](https://doi.org/10.1111/joes.12618). URL: <https://www.rug.nl/ggdc/historicaldevelopment/maddison/releases/maddison-project-database-2023>.

[50] Eli G. Rau and Susan Stokes. “Income inequality and the erosion of democracy in the twenty-first century”. In: *Proceedings of the National Academy of Sciences* 122.1 (2025), e2422543121. DOI: [10.1073/pnas.2422543121](https://doi.org/10.1073/pnas.2422543121). URL: <https://www.pnas.org/doi/abs/10.1073/pnas.2422543121>.

[51] Marten Scheffer, Jordi Bascompte, William A. Brock, Victor Brovkin, Stephen R. Carpenter, et al. “Early-warning signals for critical transitions”. In: *Nature* 461.7260 (Sept. 2009), pp. 53–59. ISSN: 1476-4687. DOI: [10.1038/nature08227](https://doi.org/10.1038/nature08227). URL: <https://doi.org/10.1038/nature08227>.

[52] Marten Scheffer, Stephen R. Carpenter, Timothy M. Lenton, Jordi Bascompte, William Brock, et al. “Anticipating Critical Transitions”. In: *Science* 338.6105 (2012), pp. 344–348. DOI: [10.1126/science.1225244](https://doi.org/10.1126/science.1225244). eprint: <https://www.science.org/doi/pdf/10.1126/science.1225244>. URL: <https://www.science.org/doi/abs/10.1126/science.1225244>.

[53] Mathieu Kessler. “Estimation of an ergodic diffusion from discrete observations”. In: *Scandinavian Journal of Statistics* 24.2 (1997), pp. 211–229.

[54] Yacine Aït-Sahalia. *Closed-form likelihood expansions for multivariate diffusions*. 2002.

[55] Andrew Gelman, John B Carlin, Hal S Stern, and Donald B Rubin. *Bayesian data analysis*. Chapman and Hall/CRC, 1995.

[56] Pierre Perron. “The great crash, the oil price shock, and the unit root hypothesis”. In: *Econometrica: journal of the Econometric Society* (1989), pp. 1361–1401.

- [57] Kenneth A Bollen. *Structural equations with latent variables*. John Wiley & Sons, 1989.
- [58] Judea Pearl. *Causality*. Cambridge university press, 2009.
- [59] Melanie Mitchell. *Complexity: A guided tour*. Oxford university press, 2009.
- [60] Karl R. Popper. *The poverty of historicism*. Boston: Beacon Press, 1957.
- [61] Ian Hacking. *The taming of chance*. 17. Cambridge University Press, 1990.
- [62] Daniel Pemstein, Kyle L. Marquardt, Eitan Tzelgov, Yi-ting Wang, Juraj Medzihorsky, et al. *The V-Dem Measurement Model: Latent Variable Analysis for Cross-National and Cross-Temporal Expert-Coded Data*. V-Dem Working Paper 21. 10th edition. Varieties of Democracy Institute, University of Gothenburg, 2025.

Appendix

A SDE Inference Methods

In this appendix, we demonstrate the methodologies employed to infer the underlying dynamics of historical trajectories. We recall the governing stochastic differential equation (SDE) introduced in the main text:

$$d\mathbf{x}_t^{(i)} = \mathbf{F}(\mathbf{x}_t^{(i)}) dt + \sqrt{2\mathbf{D}(\mathbf{x}_t^{(i)})} d\mathbf{W}_t^{(i)}, \quad (\text{S1})$$

where $\mathbf{x}_t \in \mathbb{R}^d$ denotes the system state of unit i and $\mathbf{W}_t^{(i)}$ is a standard d -dimensional Wiener process independent across units. The drift vector field $\mathbf{F} : \mathbb{R}^d \rightarrow \mathbb{R}^d$ defines the deterministic trends of the system, while the diffusion matrix $\mathbf{D} : \mathbb{R}^d \rightarrow \mathbb{R}^{d \times d}$ encodes the state-dependent noise amplitude and correlation structure. For the sake of brevity, we will omit the unit index (i) when referring to the general dynamics, unless a distinction between units is necessary. The primary objective of the SDE inference methods described below is to solve the inverse problem: inferring the unknown functions $\mathbf{F}(\mathbf{x})$ and $\mathbf{D}(\mathbf{x})$ solely from discrete, and often sparse, empirical observations. We employ two complementary approaches in this paper.

A.1 Langevin Bayesian Networks (LBN)

The Langevin Bayesian Networks (LBN) framework [14] is designed to uncover the underlying Langevin equation from observed stochastic trajectories by approximating the Kramers–Moyal coefficients via neural networks. This methodology facilitates the precise and separate inference of the drift field and diffusion matrix, and it is particularly noted for providing unbiased estimators that eliminate leading-order biases for second-order SDEs. A significant advantage of LBN is its inherent ability to provide uncertainty estimates associated with its predictions. The effectiveness and versatility of this framework have been demonstrated through various challenging scenarios, including highly nonlinear and non-stationary stochastic models such as spiking neuron models and microscopic engines in Ref. [14].

While the original LBN implementation relies on variational inference, this study incorporates Stochastic Weight Averaging-Gaussian (SWAG) [46] and k-fold cross-validation to construct a robust neural network ensemble. This multi-fold approach is essential because historical data in many stochastic systems is sparse and limited in quantity; as a result, the performance of a model using a single validation split can be highly sensitive to the specific partitioning of the data. Furthermore, neglecting a validation set entirely often leads to severe overfitting, which compromises the model’s ability to generalize to new states. By generating an ensemble of predictions, the framework provides a distribution of possible outputs rather than a single

value. The mean of these predictions defines the reference model, while the variance allows for a quantitative assessment of prediction uncertainty. The overall training procedure is summarized in Algorithm S1.

Algorithm S1 Training and Inference procedure of LBN with SWAG Ensemble

Require: LBN architectures for drift and diffusion, optimizer, dataset $\mathcal{D} \equiv \{(\mathbf{x}_t, \mathbf{y}_t)\}$ with input state \mathbf{x} and target label \mathbf{y} assigned based on the quantity to infer.

- 1: Split \mathcal{D} into k equally sized folds $\{\mathcal{D}_1, \dots, \mathcal{D}_k\}$.
- 2: **for** $i = 1$ **to** k **do**
- 3: Set $\mathcal{D}_{\text{val}} \leftarrow \mathcal{D}_i$ and $\mathcal{D}_{\text{tr}} \leftarrow \mathcal{D} \setminus \mathcal{D}_i$.
- 4: Initialize network parameters $\boldsymbol{\theta}_i$.
- 5: **loop**
- 6: Compute \mathcal{L} over \mathcal{D}_{tr} by $\mathcal{L}(\boldsymbol{\theta}_i, \mathcal{D}_{\text{tr}}) = \frac{1}{2} \langle (\mathbf{y} - \mathbf{y}_{\boldsymbol{\theta}_i}(\mathbf{x}))^2 \rangle_{\mathcal{D}_{\text{tr}}}$ with the network output $\mathbf{y}_{\boldsymbol{\theta}_i}$.
- 7: Update $\boldsymbol{\theta}_i$ via the optimizer to minimize \mathcal{L}^E .
- 8: Monitor $\mathcal{L}(\boldsymbol{\theta}_i, \mathcal{D}_{\text{val}})$ to prevent overfitting and identify the SWA start point.
- 9: **if** SWA start condition is met **then**
- 10: Update SWA running mean $\bar{\boldsymbol{\theta}}_i$ and second moment $\bar{\boldsymbol{\theta}}^2_i$ for SWAG.
- 11: **end if**
- 12: **end loop**
- 13: Construct the i -th SWAG posterior $\mathcal{P}_i(\boldsymbol{\theta} | \mathcal{D}) \approx \mathcal{N}(\bar{\boldsymbol{\theta}}_i, \boldsymbol{\Sigma}_i)$, where $\boldsymbol{\Sigma}_i$ is derived from the moments.
- 14: **end for**
- 15: Generate an ensemble of parameters $\{\boldsymbol{\theta}^{(j)}\}_{j=1}^{N_{\text{ens}}}$ by sampling N_{ens}/k parameters from each posterior \mathcal{P}_i
- 16: For a given state \mathbf{x} , compute the ensemble mean $\hat{\mathbf{y}}(\mathbf{x})$ and variance $\hat{\boldsymbol{\Sigma}}_{\mathbf{y}}(\mathbf{x})$ from the predictions of $\{\boldsymbol{\theta}^{(j)}\}$

A.1.1 Approximation of Kramers-Moyal Coefficients

To infer the drift vector field $\mathbf{F}(\mathbf{x})$ and the diffusion matrix $\mathbf{D}(\mathbf{x})$, we leverage the relationship between these functions and the conditional moments of the state transitions, known as the Kramers–Moyal coefficients [25]. In the LBN framework, we employ neural networks to approximate these expectations directly from the finite-time transition data. Specifically, the estimators for the drift and diffusion at a given state \mathbf{x}_t , denoted as $\hat{\mathbf{F}}_{\boldsymbol{\theta}}(\mathbf{x}_t)$ and $\hat{\mathbf{D}}_{\boldsymbol{\theta}}(\mathbf{x}_t)$, are formulated with trainable parameters $\boldsymbol{\theta}$ as follows:

$$\hat{\mathbf{F}}_{\boldsymbol{\theta}}(\mathbf{x}_t) = \frac{\langle \Delta \mathbf{x}_t \mid \mathbf{x}_t \rangle}{\Delta t}, \quad \hat{\mathbf{D}}_{\boldsymbol{\theta}}(\mathbf{x}_t) = \frac{\langle \Delta \mathbf{x}_t \Delta \mathbf{x}_t^\top \mid \mathbf{x}_t \rangle}{2\Delta t}, \quad (\text{S2})$$

where $\Delta \mathbf{x}_t \equiv \mathbf{x}_{t+\Delta t} - \mathbf{x}_t$ represents the state displacement over the effective time interval Δt , and $\langle \cdot \mid \mathbf{x}_t \rangle$ denotes the expectation conditional on the current state \mathbf{x}_t . This reconstruction strategy based on Kramers–Moyal coefficients is widely adopted in data-driven stochastic modeling [26, 39, 45]. In the context of the learning scheme described in Algorithm S1, Eq. (S2) defines the target labels \mathbf{y}_t for each network. For the drift network $\mathbf{F}_{\boldsymbol{\theta}}$, the target is the instantaneous velocity $\mathbf{y}_t = \Delta \mathbf{x}_t / \Delta t$. The network is trained to minimize the mean squared error between its output and this empirical velocity, effectively learning the conditional expectation $\langle (\Delta \mathbf{x}_t / \Delta t) \mid \mathbf{x}_t \rangle$. Similarly, for the diffusion network $\mathbf{D}_{\boldsymbol{\theta}}$, the target is the normalized outer product of the displacement $\mathbf{y}_t = (\Delta \mathbf{x}_t \Delta \mathbf{x}_t^\top) / (2\Delta t)$. As noted in Sec. 4, the time step Δt used here

corresponds to the rescaled simulation time (e.g., $\Delta t = 10^{-2}$) to ensure numerical stability and consistency with the continuous-time SDE formulation.

A.1.2 Network architectures

We implement the LBN framework using two distinct neural networks to model the drift vector $\mathbf{F}_\theta(\mathbf{x})$ and the diffusion matrix $\mathbf{D}_\theta(\mathbf{x})$. The drift network consists of fully connected blocks, where each block comprises a linear layer, followed by Layer Normalization and an ELU activation, and the diffusion network follows a similar architecture. A critical feature of the diffusion estimator is the enforcement of the symmetric positive semi-definite (PSD) constraint. The network outputs a vector representing the lower-triangular elements of a symmetric matrix. To ensure the PSD property, we calculate the eigen-decomposition of this symmetric form to obtain eigenvectors \mathbf{U} and eigenvalues $\boldsymbol{\lambda}$. The final diffusion matrix is then constructed by rectifying the eigenvalues:

$$\hat{\mathbf{D}}_\theta(\mathbf{x}) = \mathbf{U} \operatorname{diag}(\operatorname{Softplus}(\boldsymbol{\lambda}) + \epsilon) \mathbf{U}^\top, \quad (\text{S3})$$

where $\operatorname{diag}(\cdot)$ constructs a diagonal matrix, $\operatorname{Softplus}(z) = \ln(1 + e^z)$ is applied element-wise to enforce positivity, and $\epsilon = 10^{-9}$ is a small constant for numerical stability. This ensures that the resulting diffusion matrix is strictly PSD while remaining differentiable. Overall, we used the Adam optimizer to minimize the loss function.

A.2 Nonparametric Gaussian process SDE (npSDE)

We apply a nonparametric SDE learning framework [15], termed the *nonparametric Gaussian process SDE* (npSDE), in which both drift and diffusion functions are modeled via Gaussian processes. We adopt this method with minor adaptations to serve as our estimator for the sparse historical dataset.

A.2.1 Gaussian process priors for drift and diffusion

Following Ref. [15], we model the unknown drift and diffusion functions using sparse Gaussian Processes (GPs). For the drift vector field $\mathbf{F}(\mathbf{x})$, we place a zero-mean vector-valued GP prior:

$$\mathbf{F}(\cdot) \sim \mathcal{GP}(\mathbf{0}, \mathbf{K}_F(\cdot, \cdot)), \quad (\text{S4})$$

where $\mathcal{GP}(\mu, K)$ denotes a Gaussian process distribution with mean function μ and covariance kernel K . Here, \mathbf{K}_F is a matrix-valued kernel on $\mathbb{R}^d \times \mathbb{R}^d$ that specifies prior covariances between drift vectors at different states. In practice, we use a decomposable kernel structure $\mathbf{K}_F(\mathbf{x}, \mathbf{x}') = \mathbf{A} k_F(\mathbf{x}, \mathbf{x}')$ where k_F is a scalar

base kernel (e.g., squared exponential) with output variance and length-scale parameters, and \mathbf{A} is a positive semidefinite matrix (often set to \mathbf{I}_d) encoding dependencies between drift components. This prior encodes the assumption that nearby states have similar drift vectors, with the notion of “nearby” controlled by the kernel.

For the stochastic term, we recall that the diffusion matrix $\mathbf{D}(\mathbf{x})$ determines the noise covariance. In the npSDE method, we model this isotropic noise via a scalar amplitude field $b(\mathbf{x}) : \mathbb{R}^d \rightarrow \mathbb{R}$, such that the diffusion matrix is defined as:

$$\mathbf{D}(\mathbf{x}) = \frac{1}{2}b(\mathbf{x})^2 \mathbf{I}_d. \quad (\text{S5})$$

We place a scalar GP prior on this diffusion amplitude function:

$$b(\cdot) \sim \mathcal{GP}(0, k_b(\cdot, \cdot)), \quad (\text{S6})$$

where k_b is a scalar base kernel governing the smoothness of the state-dependent volatility.

Direct GP regression on \mathbf{F} and $b(\mathbf{x})$ is infeasible because the drift and diffusion are only indirectly related to observed data through the integration of the SDE. To address this, we utilize a sparse inducing-point parameterization. Let $Z = \{\mathbf{z}_m\}_{m=1}^M \subset \mathbb{R}^d$ be a set of M inducing locations in the state space. We introduce inducing variables for the drift and diffusion amplitude, denoted as $\mathbf{U}_F = \{\mathbf{F}(\mathbf{z}_m)\}_{m=1}^M$ and $\mathbf{U}_b = \{b(\mathbf{z}_m)\}_{m=1}^M$, respectively.

We then approximate the drift and diffusion at any arbitrary state \mathbf{x} using the GP predictive means conditioned on these inducing variables:

$$\mathbf{F}(\mathbf{x}) \approx \mathbf{K}_F(\mathbf{x}, Z)\mathbf{K}_F(Z, Z)^{-1}\mathbf{U}_F, \quad (\text{S7})$$

$$b(\mathbf{x}) \approx k_b(\mathbf{x}, Z)k_b(Z, Z)^{-1}\mathbf{U}_b, \quad (\text{S8})$$

where $\mathbf{K}_F(\mathbf{x}, Z)$, $k_b(\mathbf{x}, Z)$ denote kernel evaluations between \mathbf{x} and the inducing locations Z . With a sufficiently rich kernel and enough inducing points, these interpolants can approximate a wide range of drift and diffusion functions.

A.2.2 Simulation-based likelihood and sparse, irregular data

Let $\boldsymbol{\theta}$ collect the inducing values $(\mathbf{U}_F, \mathbf{U}_b)$, kernel hyperparameters, and observation noise variances. Given $\boldsymbol{\theta}$, the GP-interpolated functions in Eqs. (S7) and (S8) define a specific SDE and thus a distribution over paths $\mathbf{x}_{i,0:T_i}$ for each unit i . The observed data \mathbf{y}_{ik} are assumed to be generated by

$$\mathbf{y}_{ik} = \mathbf{x}_{t_{ik}}^{(i)} + \boldsymbol{\varepsilon}_{ik}, \quad \boldsymbol{\varepsilon}_{ik} \sim \mathcal{N}(\mathbf{0}, \mathbf{R}),$$

with diagonal observation noise covariance \mathbf{R} .

The marginal likelihood of the data under parameter $\boldsymbol{\theta}$,

$$\mathcal{L}(\boldsymbol{\theta}) = p(\{\mathbf{y}_{ik}\}_{i,k} \mid \boldsymbol{\theta}) = \int p(\{\mathbf{y}_{ik}\}_{i,k} \mid \{\mathbf{x}_{i,0:T_i}\}, \boldsymbol{\theta}) \prod_i p(\mathbf{x}_{i,0:T_i} \mid \boldsymbol{\theta}) d\mathbf{x}_{i,0:T_i}, \quad (\text{S9})$$

is analytically intractable for nonlinear SDEs. Instead of relying on gradient matching (which approximates the dynamics by matching empirical time derivatives and is only justified for densely sampled data), Ref. [15] approximates Eq. (S9) by simulating many sample paths from the SDE and comparing the resulting state distributions to the observed data.

Concretely, for each unit i and time interval $[t_k, t_{k+1}]$, we simulate a collection of paths using the Euler–Maruyama scheme:

$$\mathbf{x}_{t+\delta t}^{(i)} = \mathbf{x}_t^{(i)} + \mathbf{F}(\mathbf{x}_t^{(i)}) \delta t + b(\mathbf{x}_t^{(i)}) \delta \mathbf{W}_t^{(i)},$$

with a small internal step size δt that may be much finer than the observation intervals and $\delta \mathbf{W}_t^{(i)} \sim \mathcal{N}(\mathbf{0}, \mathbf{I}_d \delta t)$. Starting from the initial observed state (or an initial distribution), we propagate these paths up to each observation time and obtain Monte Carlo samples from the model-implied state distributions $p(\mathbf{x}_{t_{ik}}^{(i)} \mid \boldsymbol{\theta})$. Comparing these simulated distributions with the observed \mathbf{y}_{ik} yields a stochastic approximation to the expected log-likelihood.

In practice, this results in an objective of the form

$$\hat{\mathcal{L}}(\boldsymbol{\theta}) \approx \sum_{i,k} \log \left[\frac{1}{S} \sum_{s=1}^S \mathcal{N}(\mathbf{y}_{ik}; \mathbf{x}_{t_{ik}}^{(i,s)}, \mathbf{R}) \right] + \log P(\boldsymbol{\theta}), \quad (\text{S10})$$

where $\{\mathbf{x}_{t_{ik}}^{(i,s)}\}_{s=1}^S$ are simulated states from S independent paths for unit i , and $P(\boldsymbol{\theta})$ is the GP prior over inducing values and hyperparameters. The model learns $\boldsymbol{\theta}$ so that simulated paths produce state distributions whose noisy projections match the empirical observations, even when the observation times $\{t_{ik}\}$ are highly irregular, and the number of points per trajectory is small.

A.2.3 Sensitivity equations and gradient-based optimization

A key contribution of Ref. [15] is an efficient method for computing gradients of the Monte Carlo objective (S10) with respect to $\boldsymbol{\theta}$. Naively differentiating through the path simulation with finite differences would be prohibitively expensive. Instead, the method derives discrete-time sensitivity equations for the Euler–Maruyama updates, which express derivatives of the simulated states with respect to the inducing values and kernel parameters in closed form.

Let $\mathbf{x}_t(\boldsymbol{\theta})$ denote a simulated state at time t , and consider the Euler–Maruyama update:

$$\mathbf{x}_{t+\delta t}(\boldsymbol{\theta}) = \mathbf{x}_t(\boldsymbol{\theta}) + \mathbf{F}(\mathbf{x}_t(\boldsymbol{\theta}); \boldsymbol{\theta}) \delta t + b(\mathbf{x}_t(\boldsymbol{\theta}); \boldsymbol{\theta}) \delta \mathbf{W}_t^{(i)}. \quad (\text{S11})$$

Differentiating both sides with respect to a parameter component θ_j yields a recursion for $\partial \mathbf{x}_{t+\delta t} / \partial \theta_j$ in terms of $\partial \mathbf{x}_t / \partial \theta_j$ and the derivatives of \mathbf{F} and b with respect to both \mathbf{x} and $\boldsymbol{\theta}$. These derivatives can be computed analytically via the kernel functions used in Eqs. (S7)–(S8). The resulting sensitivity recursions are iterated in parallel with the state updates during simulation, providing pathwise gradients $\partial \mathbf{x}_{t_k}^{(i,s)} / \partial \theta_j$ for each simulated path.

Substituting these sensitivities into the gradient of Eq. (S10) yields an unbiased stochastic gradient estimator for $\nabla_{\boldsymbol{\theta}} \mathcal{L}(\boldsymbol{\theta})$, which can be used with standard gradient-based optimizers such as L-BFGS or stochastic gradient descent. Computationally, the cost of computing sensitivities is of the same order as simulating the SDE itself, making the overall procedure tractable for moderate numbers of inducing points and simulation steps.

B Dataset Description

B.1 Application 1: Evolution of Political Economy

To quantitatively describe the evolution of political economy, we construct a state space spanned by three key dimensions: political democracy, economic inequality, and economic growth. We define the state of a society at time t as a vector $\mathbf{x}(t) \equiv [x_D, x_I, x_G]^\top$. To synthesize the multidimensional nature of institutional and social indicators, we employ Principal Component Analysis (PCA) for democracy and inequality, defining x_D and x_I as the first principal component (pc_1) of their respective underlying variables. Each component is detailed as follows:

- **Democracy (x_D):** We utilize the *Varieties of Democracy* (V-Dem) dataset [47, 62] to quantify the level of democratic institutions. Specifically, we extract the PC1 from the V-Dem framework’s five high-level principles of democracy: electoral, liberal, participatory, deliberative, and egalitarian indices. This pc_1 captures approximately 97.3% of the total variance, demonstrating that these five indices are highly correlated and effectively represent a unified dimension of democratic governance.
- **Economic Inequality (x_I):** Inequality data is sourced from the *World Inequality Database* (WID) [48]. We construct x_I using the pc_1 of two complementary Gini coefficients: pre-tax national income and household wealth. The pc_1 explains 76.6% of the total variation, providing a holistic measure of

inequality that consistently tracks disparities in both income flows and accumulated wealth stocks.

- **Economic Growth (x_G):** For the aggregate economic growth, we use the real GDP per capita data from the *Maddison Project Database* (MPD) [49]. Given that economic growth spans several orders of magnitude over history, we construct x_G using the standardized value of the logarithm of real GDP per capita, $\log_{10}(\text{GDP/capita})$.

To ensure the empirical integrity of our analysis, we implemented a strict data filtering protocol. First, from the WID dataset, we excluded observations with low imputation quality (e.g., regional-level imputations) to rely solely on high-fidelity, country-specific primary sources. Second, although the raw data is structured annually, many countries exhibit missing years. While various imputation methods exist to fill such gaps, we opted not to perform any additional imputation to avoid introducing artificial trends or statistical artifacts.

The resulting dataset constitutes an unbalanced panel of 149 countries at an annual resolution, totaling 4,144 observations. The time horizon differs by nation, ranging from long-term observations (e.g., France, 1910–2022) to shorter, more recent records (e.g., Palestine-Gaza, starting in 2007). For the vast majority of countries, the indicators are consistently tracked from 1995 to 2022.

B.2 Application 2: Historical Civilizations

We utilize the *Polaris* dataset from the Seshat: Global History Databank [16]. This dataset tracks the sociopolitical characteristics of polities located in 46 Natural Geographic Areas (NGAs) distributed globally, covering a time span from the Neolithic period to the modern era. While the original database contains hundreds of variables, we project the system state into a two-dimensional latent space $\mathbf{x} = [x_S, x_C]^\top$, representing *Scale* and *Computation*, respectively.

The *Scale* dimension (x_S) captures the material magnitude of a polity. It is constructed from three key quantitative indicators: polity population, polity territory, and the population of the largest settlement. These variables are aggregated to form a continuous index representing the physical expanse and demographic size of the society. The *Computation* dimension (x_C) serves as a proxy for a society’s information processing capacity and institutional complexity. Key constituent variables include governance sophistication, information systems, infrastructure, and monetary systems. Higher values of x_C correspond to a greater capacity for information storage, processing, and administrative control.

The final dataset consists of irregular time series for 46 NGAs, totaling approximately 400 region-period observations. Unlike modern economic data, the observation intervals are sparse and uneven, typically sampled at 100-year steps, though gaps vary significantly. Consistent with our framework’s capability to handle sparse data, we utilize the raw discrete observations without performing temporal interpolation.

C Additional Results

C.1 Epistemic uncertainty in Application 1

A key advantage of LBN is that they provide not only point estimates of the drift and diffusion fields, but also *epistemic uncertainty* over the inferred dynamics. In Application 1, we quantify epistemic uncertainty using SWAG combined with k -fold cross-validation. Specifically, for each fold, we fit a SWAG network and draw an ensemble of SDE models by sampling network parameters from the corresponding approximate posterior. We then aggregate all sampled models across the k folds into a single global ensemble. At each state-space location \mathbf{x} , the mean drift/diffusion estimate is computed as the ensemble average, and uncertainty is quantified by the variability (standard deviation) across ensemble members.

For the drift field $\mathbf{F}(\mathbf{x})$ in Fig. S1, we compute a normalized epistemic uncertainty defined as

$$\sigma_{\text{epi}}(\mathbf{x}) = \frac{\text{std}[\mathbf{F}(\mathbf{x})]}{\sqrt{\mathbb{E}[\|\mathbf{F}(\mathbf{x})\|^2]}}, \quad (\text{S12})$$

where the standard deviation ($\text{std}[\cdot]$) and expectation ($\mathbb{E}[\cdot]$) are taken across the aggregated ensemble. This dimensionless ratio captures the relative uncertainty in the inferred drift magnitude. For the diffusion matrix $\mathbf{D}(\mathbf{x})$ in Fig. S2, we apply an analogous normalized uncertainty metric to the eigenvalues of $\mathbf{D}(\mathbf{x})$, in direct analogy to the drift-field definition above. Note that, because $\sigma_{\text{epi}}(\mathbf{x})$ is normalized by the local second moment, regions where $\|\mathbf{F}(\mathbf{x})\|$ (or the diffusion strength) is close to zero can exhibit large relative uncertainty even if the absolute variability is small. Such regions should be interpreted as having low signal-to-noise (i.e., the inferred magnitude is close to zero), rather than as indicating large absolute uncertainty.

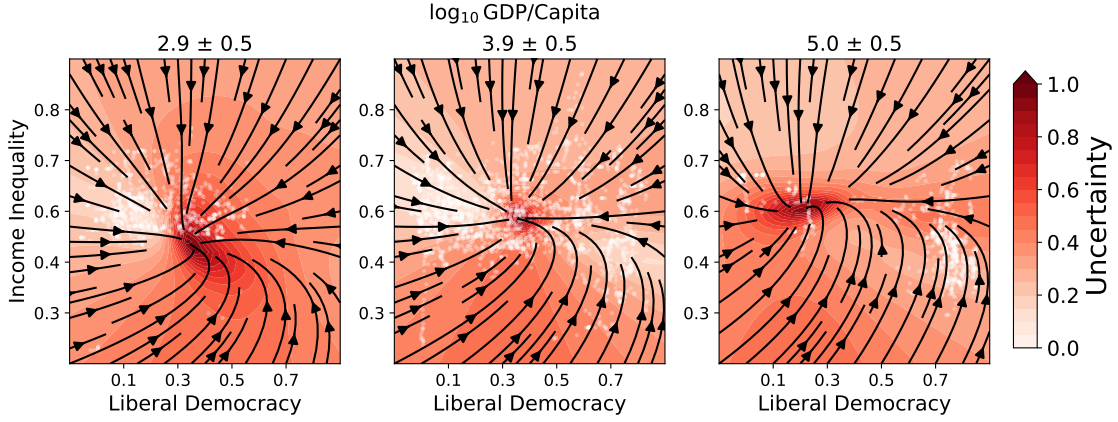


Figure S1: Uncertainty of inferred drift field $\mathbf{F}(\mathbf{x})$ on the Democracy-Inequality plane. Columns correspond to different ranges of $\log_{10}(\text{GDP/capita})$ (left to right: $2.9, 3.9, 5.0$). Black streamlines depict the mean drift field, the background color map indicates the epistemic uncertainty σ_{epi} of inferred $\mathbf{F}(\mathbf{x})$, and white dots represent the observed data points. The axes display values mapped from \mathbf{x} back to the original variable space via linear fitting for visualization. Note that σ_{epi} is a relative measure and can be large where the inferred field magnitude is close to zero.

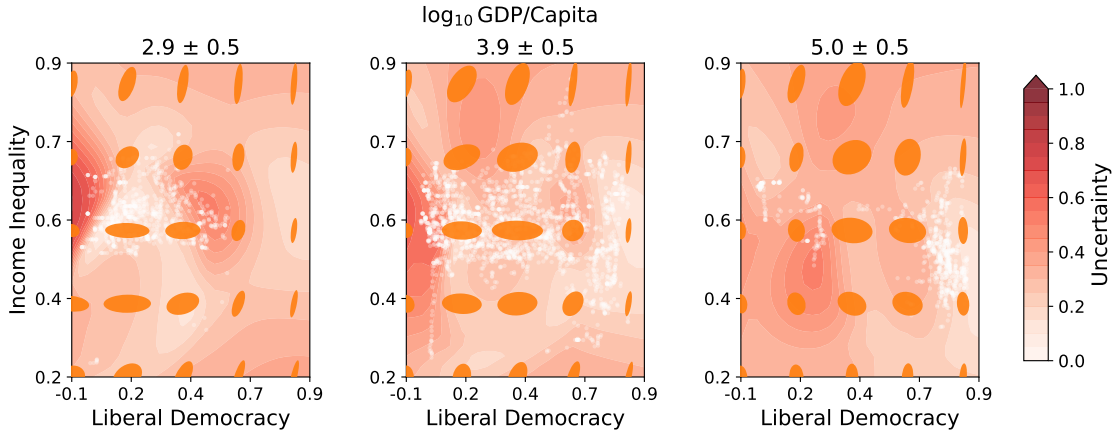


Figure S2: Uncertainty of inferred diffusion $\mathbf{D}(\mathbf{x})$ on the Democracy-Inequality plane. Columns correspond to different ranges of $\log_{10}(\text{GDP/capita})$ (left to right: $2.9, 3.9, 5.0$). Orange ellipses depict the local diffusion anisotropy, where the orientation and size correspond to the eigenvectors and eigenvalues of $\mathbf{D}(\mathbf{x})$, respectively. The background color map indicates the epistemic uncertainty σ_{epi} of inferred $\mathbf{D}(\mathbf{x})$, and white dots represent the observed data points. The axes display values mapped from \mathbf{x} back to the original variable space via linear fitting for visualization.